JOURNAL OF GEOPHYSICAL RESEARCH, VOL. 112, B11403, doi:10.1029/2006JB004807, 2007

Dynamics of continental deformation in Asia

M. Vergnolle,[1,2] E. Calais,[3] and L. Dong[3]

Received 17 October 2006; revised 14 March 2007; accepted 25 July 2007; published 8 November 2007.

[1] The relevance of plate tectonics concepts to the description of deformation of large continental areas like Asia is subject to much debate. For some, the deformation of continents is better described by rigid motion of lithospheric blocks with strain concentrated along narrow fault zones. For others, it is better described by viscous flow of a continuously deforming solid in which faults play a minor role. Discriminating these end-member hypotheses requires spatially dense measurements of surface strain rates covering the whole deforming area. Here we revisit the issue of the forces and rheological structure that control present-day deformation in Asia. We use the "thin sheet" theory, with deformation driven by the balance of boundary and buoyancy stresses acting on a faulted lithosphere with laterally varying strength. Models are validated against a recent, homogeneous, GPS velocity field that covers most of Asia. In the models, deformation in compressional areas (Himalayas, Tien Shan, Altay) is well reproduced with strong coupling at the India/Eurasia plate contact, which allows for boundary forces to transfer into Asia. Southeastward motions observed in north and south China, however, require tensional, oceanward directed stresses, possibly generated by gravitational potential energy gradients across the Indonesian and Pacific subductions. Model and observed strain rates show that a large part of Asia undergoes no resolvable strain, with a kinematics apparently consistent with block- or plate-like motions. Internal strain, possibly continuous, is limited to high-elevation, mechanically weaker areas. Lateral variations of lithospheric strength appear to control the style of deformation in Asia, with a dynamics consistent with the thin sheet physical framework.

Citation: Vergnolle, M., E. Calais, and L. Dong (2007), Dynamics of continental deformation in Asia, *J. Geophys. Res.*, *112*, B11403, doi:10.1029/2006JB004807.

1. Introduction

[2] The success of plate tectonics is due, for a large part, to its ability to correctly describe horizontal surface motions for most of our planet by simple rotations of a limited number of rigid plates. Indeed, geodetic measurements of the relative motion of sites located far enough away from plate boundaries show a remarkable agreement with the theory [*Robbins et al.*, 1993; *Argus and Heflin*, 1995], and with only rare exceptions, the oceanic parts of plates do not deform significantly. In the continents, however, the relevance of plate tectonic concepts to describe horizontal motions remains debated [e.g., *Molnar et al.*, 1973; *Molnar and Tapponnier*, 1975; *Thatcher*, 2003; *England and Molnar*, 2005]. Seismicity is diffuse and geologic structures show that deformation can affect broad areas, suggesting more complex processes than in the oceans. For some, deformation of continents is localized on a limited number of major faults bounding rigid lithospheric blocks and is driven solely by stresses due to the motions of neighboring plates. For others, deformation is pervasive and driven, for a significant part, by buoyancy forces resulting from lateral variations of crustal thickness.

[3] Conceptual models of continental deformation in Asia follow this bimodal pattern. Edge-driven models (implicitly assuming plane strain) argue that boundary stresses due to the India-Eurasia collision are responsible for the eastward extrusion of rigid lithospheric blocks bounded by fast slipping lithospheric-scale faults [e.g., *Tapponnier et al.*, 1982; *Peltzer and Saucier*, 1996]. *Peltzer and Saucier* [1996] used these assumptions to numerically simulate the deformation of Asia and found a good fit to geological data and to the sparse geodetic observations available at the time. On the other hand, thin sheet models (implicitly assuming plane stress) treat the lithosphere as a continuous viscous medium where deformation is accommodated by crustal thinning or thickening. The resulting spatial variations in crustal thickness induce lateral variations in gravitational potential energy (GPE) that, in turn, contribute to the force balance driving deformation [*Frank*, 1972; *Molnar and Tapponnier*, 1978; *Vilotte et al.*, 1982; *England and Houseman*, 1986; *Cobbold and Davy*, 1988; *Houseman and England*, 1986, 1993]. For instance, *England and Molnar* [1997a] claim that a model in which horizontal gradients of

[1]Géosciences Azur, UMR 6526, CNRS, University of Nice, Valbonne, France.
[2]Now at Laboratoire de Géophysique Interne et Tectonophysique, UMR 5559, CNRS, Grenoble, France.
[3]Department of Earth and Atmospheric Sciences, Purdue University, West Lafayette, Indiana, USA.

0148-0227/07/2006JB004807$09.00

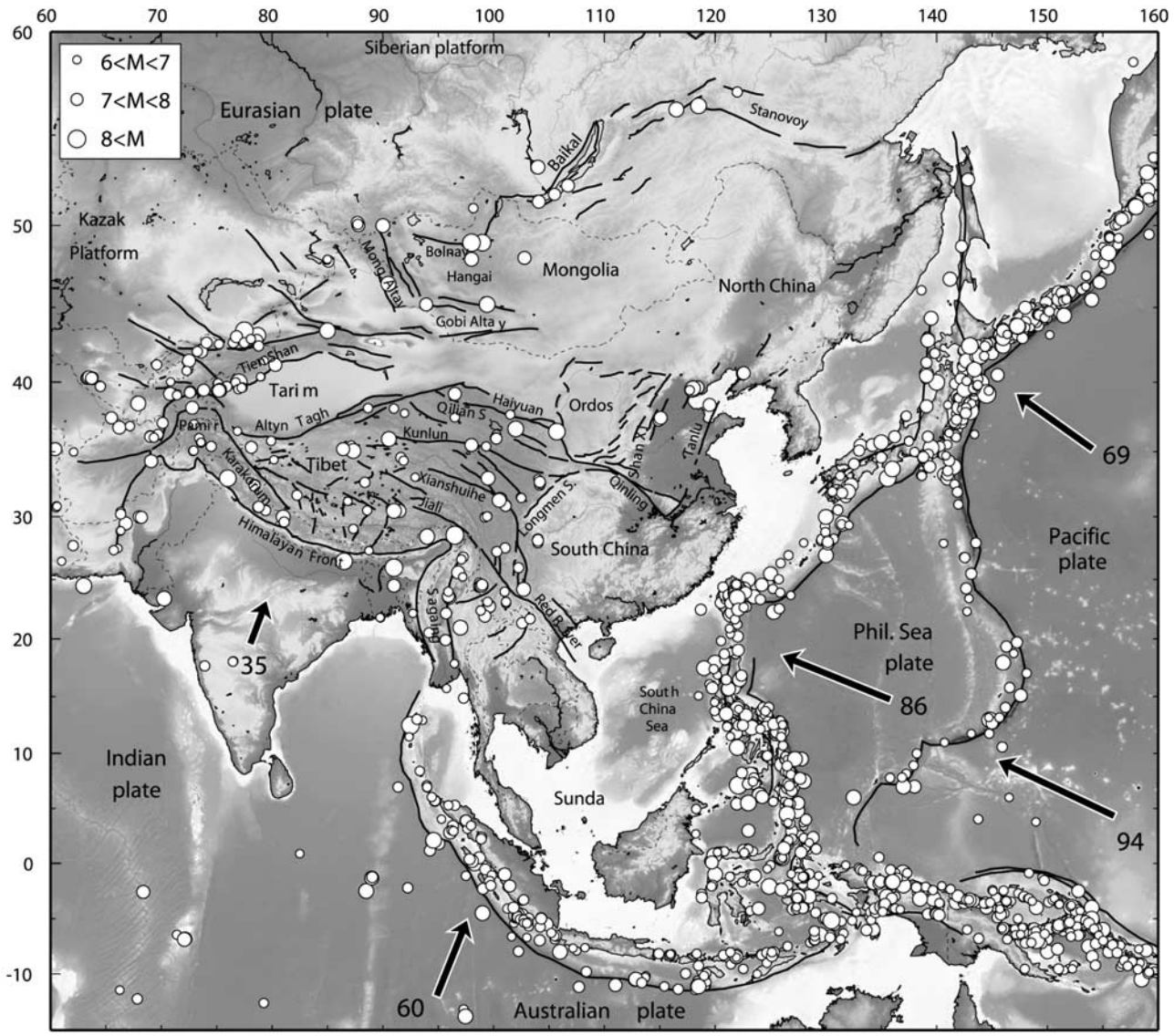

Figure 1. Topography, main active faults (black lines), seismicity (National Earthquake Information Center catalog, 1973 to Present, M > 6, depth <80 km), relative plate motions with respect to Eurasia (*Sella et al.* [2002], values at arrow tails are in mm a^{-1}), and index of the geographical names used in this paper.

the deviatoric stress required to deform a thin viscous sheet are balanced by horizontal GPE gradients explains first-order active deformation features in and around Tibet. Using a similar approach with the added constraint of a sparse GPS data set, *Flesch et al.* [2001] argue that GPE contributes to about 50% of the force balance driving present-day deformation in Asia.

[4] While the advances made in modeling continental deformation in Asia during the past 20 years have been impressive, these studies have suffered from limited quantitative data to compare theoretical predictions against. Geodetic measurements are now providing a wide-aperture image of present-day surface displacements in Asia with precision of 1–2 mm a^{-1} [e.g., *Wang et al.*, 2001; *Calais et al.*, 2006]. This, coupled with the physical framework developed by *Houseman and England* [1986] and later modified by *Bird* [1989], allows us to revisit the issue of the forces and lithospheric rheology that control present-day deformation in Asia.

2. Active Deformation in Asia

[5] Active deformation in Asia has been extensively studied over the past 30 years from tectonic [e.g., *Tapponnier and Molnar*, 1979; *Burchfiel and Royden*, 1991; *Zhang et al.*, 1995], seismological [e.g., *Molnar et al.*, 1973; *Molnar and Deng*, 1984], and geological or paleoseismological observations [e.g., *Ritz et al.*, 1995, 2003; *Mériaux et al.*, 2004; *Lacassin et al.*, 2004]. It is well established that current deformation is distributed over a broad area extending from the Himalayas in the south to the Baikal rift to the north, and from the Pamir-Tien Shan to the west to the peri-Asiatic oceanic subduction to the east (Figure 1). Seismicity is widespread and, although most earthquakes occur at the

Pacific subduction, a number of large events have also struck the interior of the continent, such as four M_w8.0–8.4 earthquakes in Mongolia between 1905 and 1957 [*Khilko et al.*, 1985; *Okal*, 1977; *Baljinnyam et al.*, 1993] or, more recently, a M_w7.4 event in the Russian Altay (September 2003 [*Bourtchevskaia et al.*, 2005]).

[6] The analysis of Landsat imagery in the late 1970s [*Molnar and Tapponnier*, 1975; *Tapponnier and Molnar*, 1977, 1979], together with geologic and seismological data [e.g., *Molnar and Deng*, 1984; *Molnar et al.*, 1987], led to the idea that Quaternary deformation in Asia was accommodated by slip on a limited number of large faults bounding aseismic, therefore assumed to be nondeforming, blocks (Tarim basin, south China, north China, Sunda; Figure 1). The boundaries of these blocks include large strike-slip faults (e.g., Altyn Tagh, Karakorum, Kunlun, Xianshuihe, Jiali, Haiyuan, Gobi Altay; Figure 1) as well as compressional ranges (e.g., Himalayas, Pamir-Tien Shan, Mongolian Altay, Gobi Altay; Figure 1). In addition to these localized deformation zones, two broad high elevation areas, the Tibetan and Mongolian plateaus, characterize the long-wavelength topography of Asia, with average elevations of 5,000 and 2,500 m and crustal thicknesses up to 70 and 50 km, respectively. The mechanism that led to such amounts of crustal thickening over broad areas and their impact on present-day deformation are still debated.

[7] The past decade has seen a rapid increase in geodetic results in Asia [e.g., *Abdrakhmatov et al.*, 1996; *Bilham et al.*, 1997; *King et al.*, 1997; *Paul et al.*, 2001; *Calais et al.*, 1998; *Heki et al.*, 1999; *Chen et al.*, 2000; *Shen et al.*, 2000; *Kogan et al.*, 2000; *Calais and Amarjargal*, 2000; *Bendick et al.*, 2000; *Shen et al.*, 2001; *Wang et al.*, 2001; *Michel et al.*, 2001; *Bock et al.*, 2003; *Calais et al.*, 2003; *Wright et al.*, 2004; *Chen et al.*, 2004; *Wallace et al.*, 2004; *Socquet et al.*, 2006]. In some instances, these studies provide important insight into the dynamics of continental deformation in Asia. For instance, GPS and interferometric synthetic aperture radar data show that the central part of the Altyn Tagh fault accumulates strain at a rate of 9 mm a^{-1} [*Bendick et al.*, 2000; *Shen et al.*, 2001; *Wallace et al.*, 2004; *Wright et al.*, 2004], inconsistent with edge-driven block models that require slip rates at least a factor of two larger [*Peltzer and Saucier*, 1996]. On the other hand, geodetic measurements of the eastward velocity of south China at 8–10 mm a^{-1} [e.g., *Wang et al.*, 2001] match block models and continuous deformation models equally well [*Peltzer and Saucier*, 1996; *Molnar and Gibson*, 1996] but proved wrong early models of extrusion that required at least 10–15 mm a^{-1} of eastward motion of south China [*Avouac and Tapponnier*, 1993]. At a continent-wide scale, *Flesch et al.* [2001] showed that GPS data and Quaternary fault were consistent with large parts of Asia undergoing little internal strain. *England and Molnar* [2005], using similar data but a different spatial resampling of the GPS velocities, argue that continuous deformation, driven for a large part by gravitational potential energy (GPE) gradients, dominate. Therefore, even though it is now accepted that only 20 to 30% of India-Eurasia convergence is accommodated by lateral extrusion of continental blocks [e.g., *Peltzer and Saucier*, 1996; *England and Molnar*, 1997b], no consensus has yet been reached on the processes and relative importance of the forces that drive present-day continental deformation in Asia.

[8] Here, we use a new GPS velocity field derived from a geodetic combination of three solutions in a consistent reference frame [*Calais et al.*, 2006] that provides horizontal motions at 165 sites in Asia with reasonably even station spacing (Figure 2). We refer the reader to *Calais et al.* [2006] for a complete description of the data analysis procedure and kinematic implications. This velocity field shows (1) unresolvable strain rates ($<3 \times 10^9$ a^{-1}) over a large part of Asia, with current motions well described by the rigid rotation of a limited number of microplates (north China, south China, Tarim basin, Sunda), and (2) internal strain, possibly continuous, limited to high-elevation areas. Many of the prominent features previously reported by local geodetic studies and predicted by deformation models are present, in particular the NNE-SSW shortening between India and the Tarim basin, accommodated by the eastward motion of Tibet and south China and the clockwise rotation of eastern Tibet around the eastern Himalayan syntaxis, and the NNW-SSE shortening across the Tien Shan at $\sim$20 mm a^{-1} in the west, decreasing eastward to $\sim$10 mm a^{-1}. The eastward to southeastward velocities observed in Mongolia and north China are, however, not reproduced by most deformation models of Asia, whether extrusion-based or thin sheet-based. Also, GPS data show that the Baikal rift zone is currently opening at 4 ± 1 mm a^{-1} [*Calais et al.*, 1998], whereas an extrusion model predicts 0–1 mm a^{-1} [*Peltzer and Saucier*, 1996]. Finally, GPS data in China show a low shortening rate across the eastern border of the Tibetan Plateau (<3 mm a^{-1} [*Chen et al.*, 2000; *Shen et al.*, 2000]), but 5–11 mm a^{-1} of far-field convergence between eastern Tibet and south China [*Shen et al.*, 2000; *Wang et al.*, 2001]. This result is at odds with extrusion models, in which the eastward motion of south China is driven by the extrusion of Tibet in response to India-Eurasia collision. As proposed by *King et al.* [1997], this absence of significant shortening across the eastern Tibetan margin might indicate that the Tibetan crust is actually rotating clockwise around the east Himalayan syntaxis, in agreement with southward velocities observed in southwestern China. In that interpretation, the eastward motion of south China is occurring independently of the motion of Tibet.

[9] Discrepancies between previous models (with very few GPS data at their disposal) and recent GPS observations may arise from the choice of (1) boundary conditions, (2) sources of deviatoric stresses (boundary versus buoyancy forces, mantle tractions), or (3) lithospheric rheology. To investigate these issues, we model present-day deformation in Asia using a finite element code that simulates the deformation of a faulted lithosphere on a spherical Earth. Deformation is driven by the balance of boundary stresses resulting from current plate motions and interplate coupling, and buoyancy stresses caused by horizontal gradients of gravitational potential energy. These stresses act on a faulted lithosphere with a vertically integrated rheology consistent with laboratory rock experiments and regional heat flow data. Model outputs are horizontal surface velocities and fault slip rates, which we

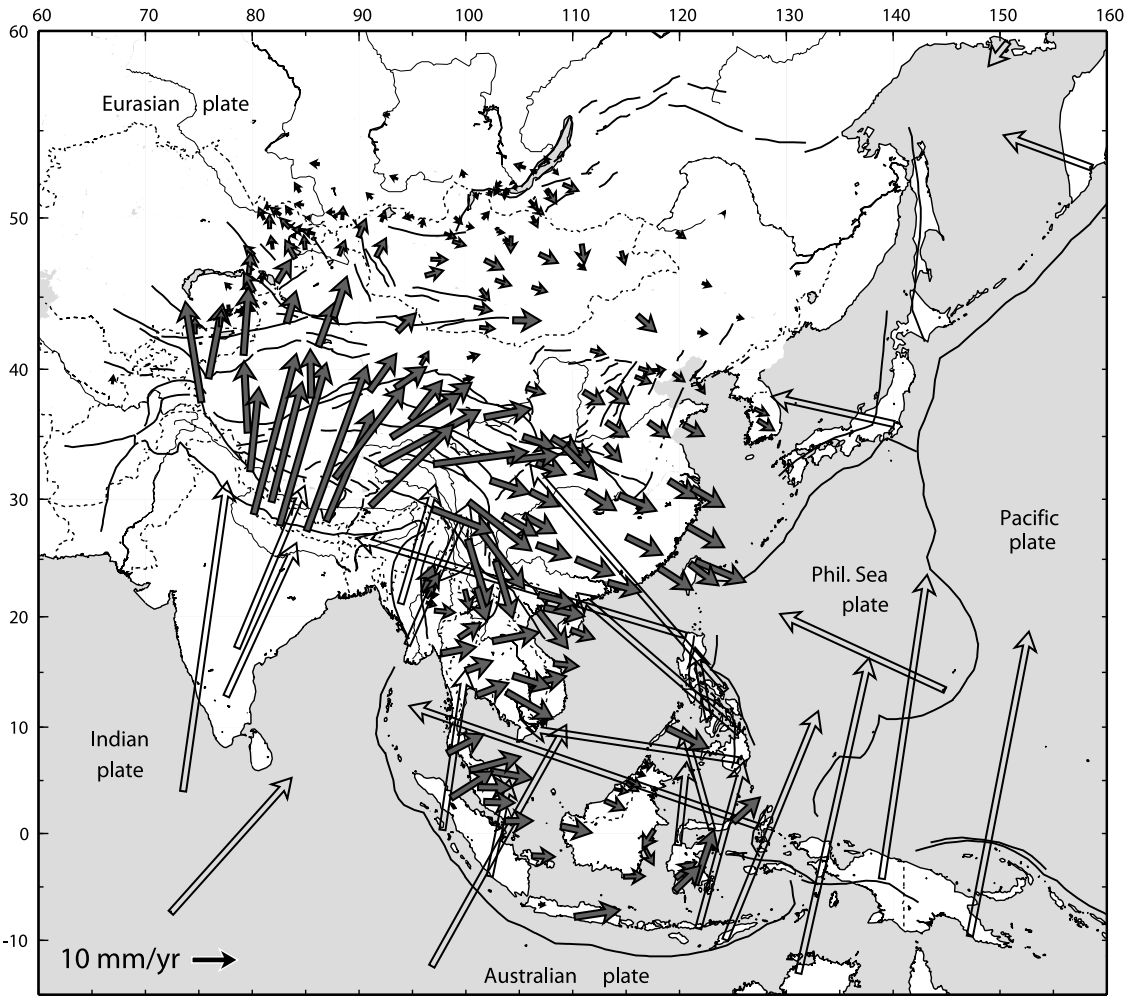

Figure 2. GPS velocities with respect to Eurasia. Only sites with velocity uncertainty less than 1.5 mm a^{-1} (95% confidence) are used and shown here. Solid arrows show GPS site velocities within Asia; open arrows show velocity of neighboring plates.

compare with corresponding observations from GPS and Quaternary geology.

3. Deformation Model

3.1. Model Assumptions

[10] We use the finite element code "SHELLS", which has previously been applied to modeling active deformation in intraplate and interplate settings in Asia, Alaska, California, Mediterranean, and New Zealand [*Bird and Baumgardner*, 1984; *Bird and Kong*, 1994; *Bird*, 1996; *Kong and Bird*, 1996; *Jiménez-Munt et al.*, 2001, 2003; *Liu and Bird*, 2002a]. We refer the reader to *Bird* [1989], *Kong and Bird* [1995], and *Bird* [1999] for a complete description of its physical basis and assumptions. We summarize hereafter its major characteristics.

[11] SHELLS approximates the lithosphere as a spherical shell of variable thickness, where the horizontal components of the momentum equation are radially integrated and velocities are constant with depth ("thin plate" approximation). Calculations are iterated until quasi-steady state is reached, using time-invariant boundary conditions, so that elasticity contributes negligibly to the strain rate. SHELLS assumes incompressibility, which is consistent with neglecting elastic strain. It uses an anelastic rheology with frictional sliding on faults in the upper crust and upper part of the lithospheric mantle, and a non-Newtonian, thermally activated dislocation creep for the lower crust and the lower part of the lithospheric mantle. SHELLS assumes two sets of constant thermal parameters for the crust and the mantle and accounts for spatial variations of surface heat flow, which is interpolated from actual measurements. Hence SHELLS simulates a layered continental lithosphere similar to the classical view derived from rock physics experiments and seismological observations, where a weak (ductile) lower crust overlies a strong upper mantle [*Brace and Kohlstedt*, 1980; *Chen and Molnar*, 1983; *Kirby and Kronenberg*, 1987]. The strength of the lithosphere is determined by 3D numerical integrals that take into account spatial variations of geotherm, crust and mantle properties, and strain rates. SHELLS does not account for flexural strength (no vertical shear traction on vertical planes), which implies that vertical normal stress is lithostatic at all points of the model. The lithosphere is divided into triangular elements and the horizontal components of velocities are solved at all the nodes. These velocities are

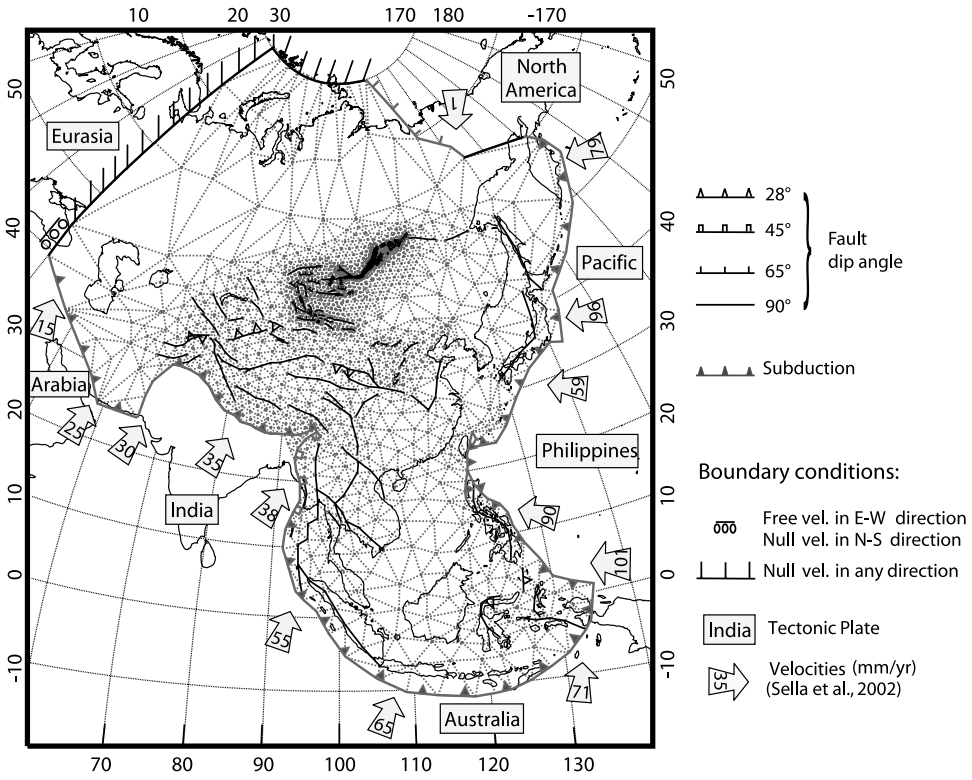

Figure 3. Finite element grid, boundary conditions, and faults used in the models.

averaged over longer time than that of the seismic cycle and the computation ignores all accelerations except gravity.

3.2. Grid Geometry and Boundary Conditions

[12] We built a finite element grid made of 2313 nodes and 3336 triangular elements (Figure 3). We densified it in the Mongolia-Baikal area for the purpose of a detailed comparison with recent geodetic results in this area [*Calais et al.*, 2003]. Since we use the Eurasian plate as a reference, we impose zero displacement along the northern and most of the western borders of the model. We allow for north-south displacements along the southernmost part of its western border, corresponding to the Zagros orogeny (Figure 3). The other grid borders follow major plate boundaries, along which we use velocity boundary conditions taken from the REVEL plate kinematic model [*Sella et al.*, 2002]. REVEL velocities agree within 1–2 mm a^{-1} with those used here for sites on plate interiors (in particular in India), and therefore provide boundary conditions consistent with the GPS velocity field used in this study.

[13] The Arabia-Eurasia plate boundary follows the main thrust zone of the Zagros orogeny and the Makran oceanic subduction. The India-Eurasia plate boundary follows the left-lateral strike-slip fault zones of Pakistan, the Himalayan frontal thrust, the right-lateral strike-slip fault system of Burma (Sagaing)-Andaman. The Australian-Eurasia boundary follows the oceanic subduction of the Australia plate under Sumatra and the Indonesian arc, with the Sorong and Palu strike-slip faults and the north Sulawesi and Moluccu subductions accounted for. The Philippines-Eurasia plate boundary follows the subduction of the Philippines Sea plate under the Philippines Archipelago and includes the Philippines strike-slip fault and the subduction reversal of the Manilla trench, in continuation with the Taiwan orogeny and further north with the Ryu-Kyu and Nankai subductions. The Pacific-Eurasia plate boundary follows the Japan, Kuriles, and Kamchatka subductions and accounts for the Main Seismic Line in Japan and the Kuriles strike-slip fault zones. The Eurasia–North America plate boundary follows the Nansen ridge.

3.3. Faults

[14] We used the trace of major active faults in Asia as reported by *Sherman* [1978], *Houdry* [1994], *Levi et al.* [1995], *Moore et al.* [1997], and *Agar and Klitgord* [1995] for the Altay-Sayan-Baikal-Stanovoy area, from *Schlupp* [1996] for Mongolia, *Tapponnier and Molnar* [1977]; *Tapponnier et al.* [1982], and from *Replumaz* [1999] for the rest of Asia (Figure 3). We assigned a single dip angle value for each type of fault: 65° for normal faults, 30° for thrust faults, 90° for strike-slip faults, and 45° for faults whose dip and sense of slip is uncertain. The dip angle for the oceanic and continental subductions at plate boundaries is 23°. The faults are free to slip in any direction, regardless of their dip angles, except for faults dipping 90°, which are forced to move in a strike-slip sense. Slip on faults is continuous and controlled by the deviatoric stress in their vicinity and by a single fault friction coefficient for the entire model. Continuous elements in the model are distinguished from faults by their higher internal friction coefficient.

[15] In order to simulate mechanical coupling between plates, we limit shear traction at convergent boundaries to a maximum value above which slip occurs. Imposing a high maximum shear traction results in large stresses to be transferred to the continent (high coupling). The opposite

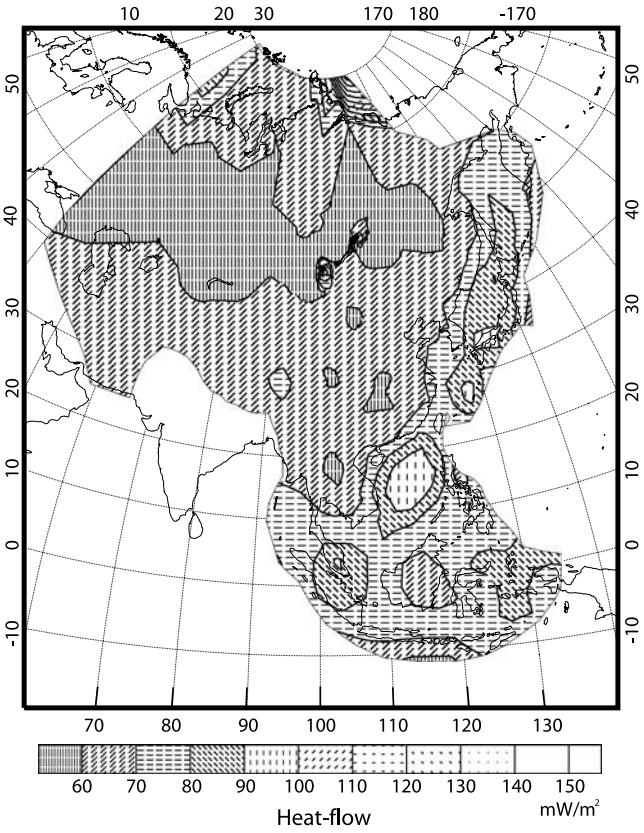

Figure 4. Map of surface heat flow used in the models. Heat flow data come from the worldwide database compiled by *Pollack et al.* [1993] and from *Lysak* [1992] for the Mongolia-Baikal area, resampled and interpolated on a 5° × 5° grid for most of the study area, except in the Mongolia-Baikal area, where we used a 12′ × 12′ grid.

is true when imposing a low maximum shear traction (low coupling). The model accounts for two maximum shear traction values, one for continental subductions (India, Arabia), one for oceanic subductions (Australia, Philippines, Pacific).

3.4. Lithospheric Structure

[16] We extracted topography and bathymetry from the ETOPO5 global database, resampled at the model nodes using a piecewise-planar interpolation. We used heat flow data from the worldwide database compiled by *Pollack et al.* [1993], and from *Lysak* [1992] for the Mongolia-Baikal area (Figure 4), also resampled at the model nodes using a piecewise-planar interpolation. Heat flow in continental Asia ranges between 50 and 80 mW m^{-2}, with most values comprised between 60 and 70 mW m^{-2}, except for two positive anomalies in the Hovsgol area (northern Mongolia) and the northern part of the Baikal rift zone, where heat flow reaches 100 and 120 mW m^{-2}, respectively.

[17] Once elevation and heat flow values are attributed to each grid node, crust and lithospheric mantle thicknesses are computed iteratively until isostasy is established and a given temperature (typically 1200 or 1300°C) is reached at the base of the lithosphere. Hence the resulting lithospheric structure (and consequently its integrated strength) depends on thermal parameters (thermal conductivity, radioactive heat production, and volumetric thermal expansion coefficient for both the crust and the mantle) and on the crust and mantle density. A broad range of thermal parameters have been proposed in the literature for continental lithosphere. We chose to test two different parameter sets, one corresponding to a weak lithosphere [*Bird*, 1998; *Liu and Bird*, 2002b], the other corresponding to a strong one (*Kong and Bird* [1996]), as summarized in Table 1.

3.5. Constitutive Laws

[18] The model considers two constitutive laws, a frictional sliding for the upper crust and the upper part of the lithospheric mantle, a non-Newtonian thermally activated dislocation creep law for the lower crust and the lower part of the lithospheric mantle, respectively given by

$$\sigma_s = \mu(-\sigma_n - P_p) \tag{1}$$

and

$$\sigma_s = A\dot{\varepsilon}^{1/n} e^{\left(\frac{B+Cz}{T}\right)} \tag{2}$$

where μ is the friction coefficient, P_p the hydrostatic pore pressure, σ_s and σ_n the shear and normal stresses, $\dot{\varepsilon}$ the strain rate, n the power law exponent, T the absolute temperature, z the depth, and A, B, and C three rheological constants, distinct for the crust and for the lithospheric mantle. Values for A, B, and C are taken from *Bird and Kong* [1994] and *Kirby* [1983], and are summarized in Table 2. Laboratory-derived power law exponents for lower crustal and upper mantle rocks usually range from 2.5 to 4 [*Kirby and Kronenberg*, 1987]; we used $n = 3$. Friction coefficients for faulted and nonfaulted elements will be derived from a parameter space search constrained by the observed GPS velocities (see below). The set of parameters chosen here, combined with the rheological laws given above, result in a factor of 2 difference in integrated strength between the weak and strong lithosphere models (Figure 5).

Table 1. Model Parameters Used To Calculate Crustal and Lithospheric Thicknesses[a]

	Weaker Rheology		Stronger Rheology	
Parameters	Crust	Mantle	Crust	Mantle
Average density at $P = 0$ and $T = 0$, kg m^{-3}	2816	3330	2816	3330
Temperature at the base of the lithosphere, °C		1200		1300
Coefficient of volumetric thermal expansion, K^{-1}	2.4×10^{-5}	3.94×10^{-5}	2.4×10^{-5}	3.1×10^{-5}
Thermal conductivity, W m^{-1} K^{-1}	2.70	3.20	3.50	5.10
Radioactive heat production, W m^{-3}	7.27×10^{-7}	3.2×10^{-8}	4.6×10^{-7}	negligible

[a]From *Bird* [1998] and *Liu and Bird* [2002b] for the weaker rheology and from *Kong and Bird* [1996] for the stronger rheology tested here.

Table 2. Non-Newtonian Dislocation Creep Law Parameters Used in the Models[a]

Parameters	Crust	Lithospheric Mantle
A, Pa $s^{1/n}$	2.3×10^9	9.5×10^{4b}
B, K	4000	18314
C, K m^{-1}	0	0.0171
σ_s^{max}, MPa	500	500

[a]These parameters are based on previous deformation modeling in California [*Bird and Kong*, 1994] and Alaska [*Bird*, 1996] for the crust and on experiments on olivine deformation for the mantle [*Kirby*, 1983].
[b]$A = 5.4 \times 10^4$ Pa $s^{1/n}$ for the stronger rheology.

3.6. Crustal and Lithospheric Thicknesses

[19] Given a set of thermal and rheological parameters, present-day topography, and surface heat flow, crustal and lithospheric thicknesses are calculated assuming isostasy and a steady state thermal regime. Resulting lithospheric and crustal thicknesses (Figure 6) match well estimates from geophysical data over most of Asia [*Villaseñor et al.*, 2001; *Li and Mooney*, 1998; *Mooney et al.*, 1998; *Lebedev and Nolet*, 2003; *Artemieva and Mooney*, 2001].

[20] Model crustal thickness ranges between 30 and 40 km for most of continental Asia, but reaches 50 and 75 km under the Mongolian and Tibetan plateaus, respectively (Figure 6). It is generally less for the weaker than for the stronger lithosphere tested here. Crustal thickness is better reproduced with a weaker lithosphere for mountain areas and high-elevation plateaus, where the stronger lithosphere results in slightly overestimated values. The opposite is true for oceanic and cratonic areas, where the stronger lithosphere matches observed crustal thicknesses slightly better than the weaker one.

[21] Model lithospheric thickness varies from 100 to 160 km for the stronger lithosphere tested here (assuming a basal temperature of 1300°C) and match values estimated by *Artemieva and Mooney* [2001] from observational data, except under the Siberian craton where model values are underestimated by about 20 km. For the case of a weaker lithosphere, model thicknesses (assuming a basal temperature of 1200°C) are usually underestimated by about 40 to 50 km compared to observations, except under Tibet where they match *Artemieva and Mooney*'s [2001] results well. Uncertainties in the estimation of lithospheric thickness from observational data are, however, large (up to 50 km) because of uncertainties in thermal parameters, temperature at the base of the lithosphere, and surface heat flow. We found that variations in lithospheric thickness of that order have a negligible effect on its integrated strength, which is primarily sensitive to crustal thickness in the models.

4. Best Fit Rheological Parameters

4.1. Parameters Tested

[22] In a first step, we seek to determine appropriate values for the internal and fault friction coefficients and for the maximum shear tractions at oceanic and continental subductions. To do so, we run a series of models that systematically explore this four-parameter space and score them using the root-mean-square (RMS) misfit of model to observed horizontal velocities. Scoring only includes sites with velocity uncertainties less than 1.5 mm a^{-1} (95% confidence). We perform this grid search for both the weak and strong lithospheres tested here and retain the set of parameters that results in the smallest RMS.

[23] We tested internal friction coefficient values (f_i) in the 0.5–0.9 range, according to standard values derived from rock physics experiments [e.g., *Byerlee*, 1978]. A number of mechanical and thermal approaches [e.g., *Cattin*, 1997; *Cattin et al.*, 1997] or modeling results [e.g., *Bird and*

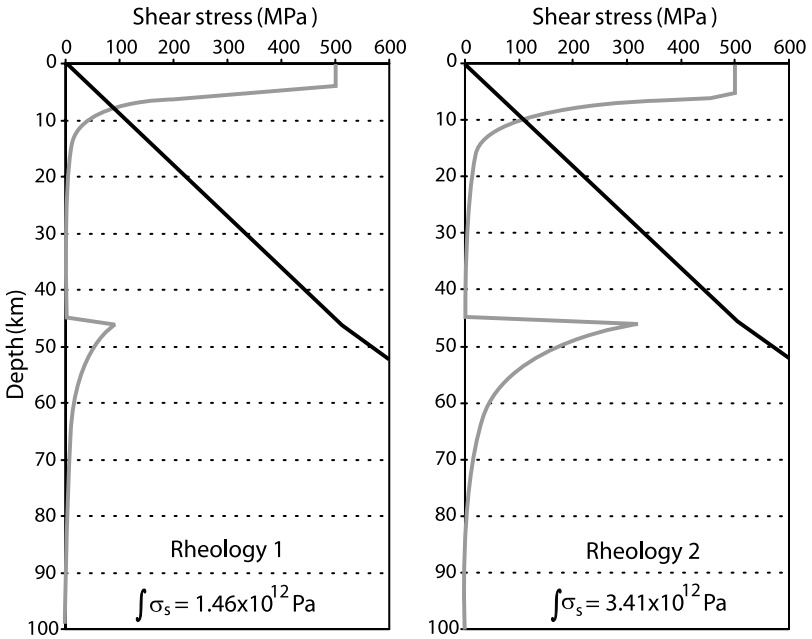

Figure 5. Examples of rheological profiles for a 45 km thick crust and a 0.059 W m^{-2} surface heat flow obtained using the thermal parameters listed in Table 1, with $\mu = 0.85$, and $\dot{\varepsilon} = 3 \times 10^{-16}$ s^{-1}. Black line shows frictional sliding; grey line is for non-Newtonian thermally activated dislocation creep.

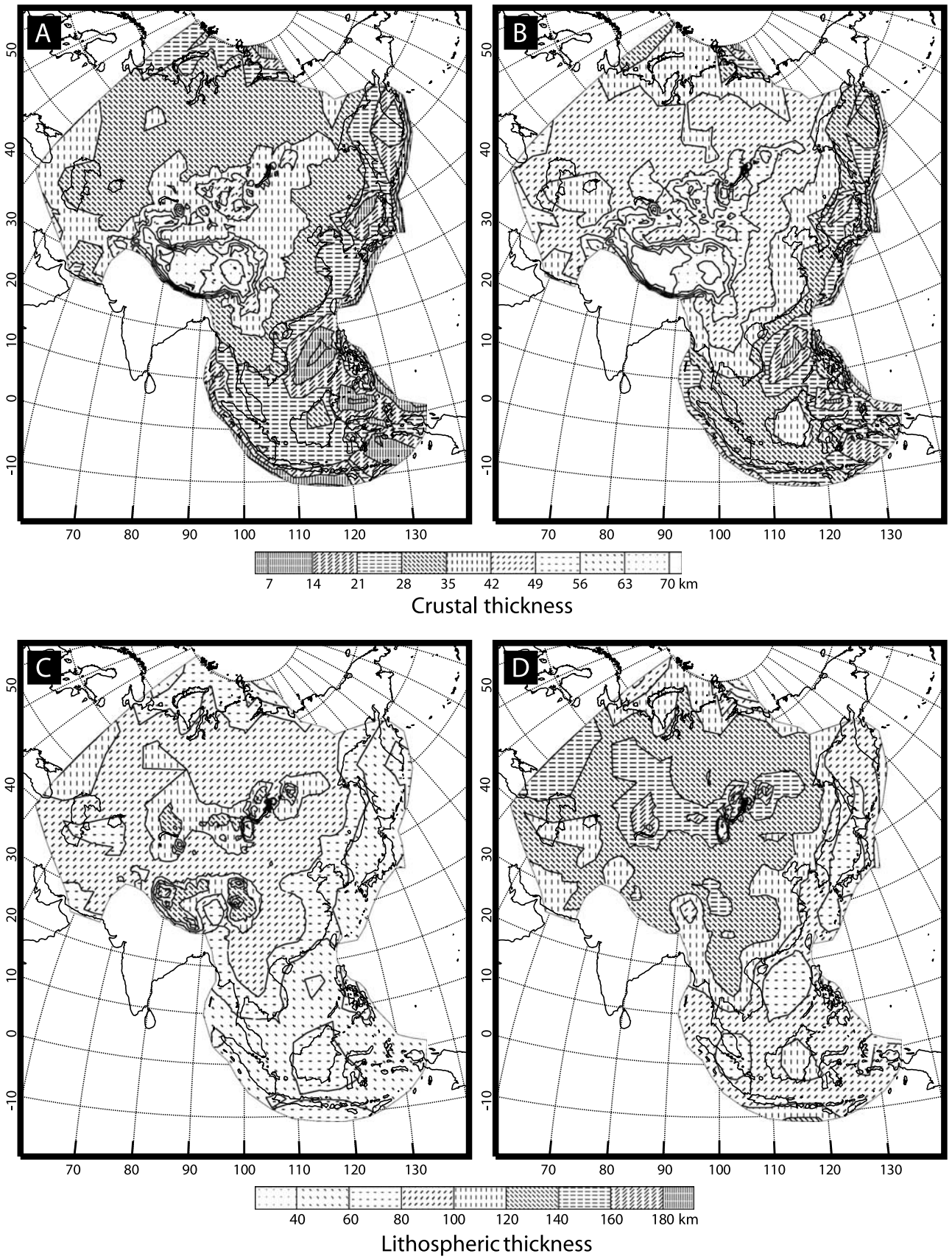

Figure 6. Crustal and lithospheric thicknesses derived from the two sets of thermal parameters tested here: (a and c) from the weaker rheology, (b and d) from the stronger rheology.

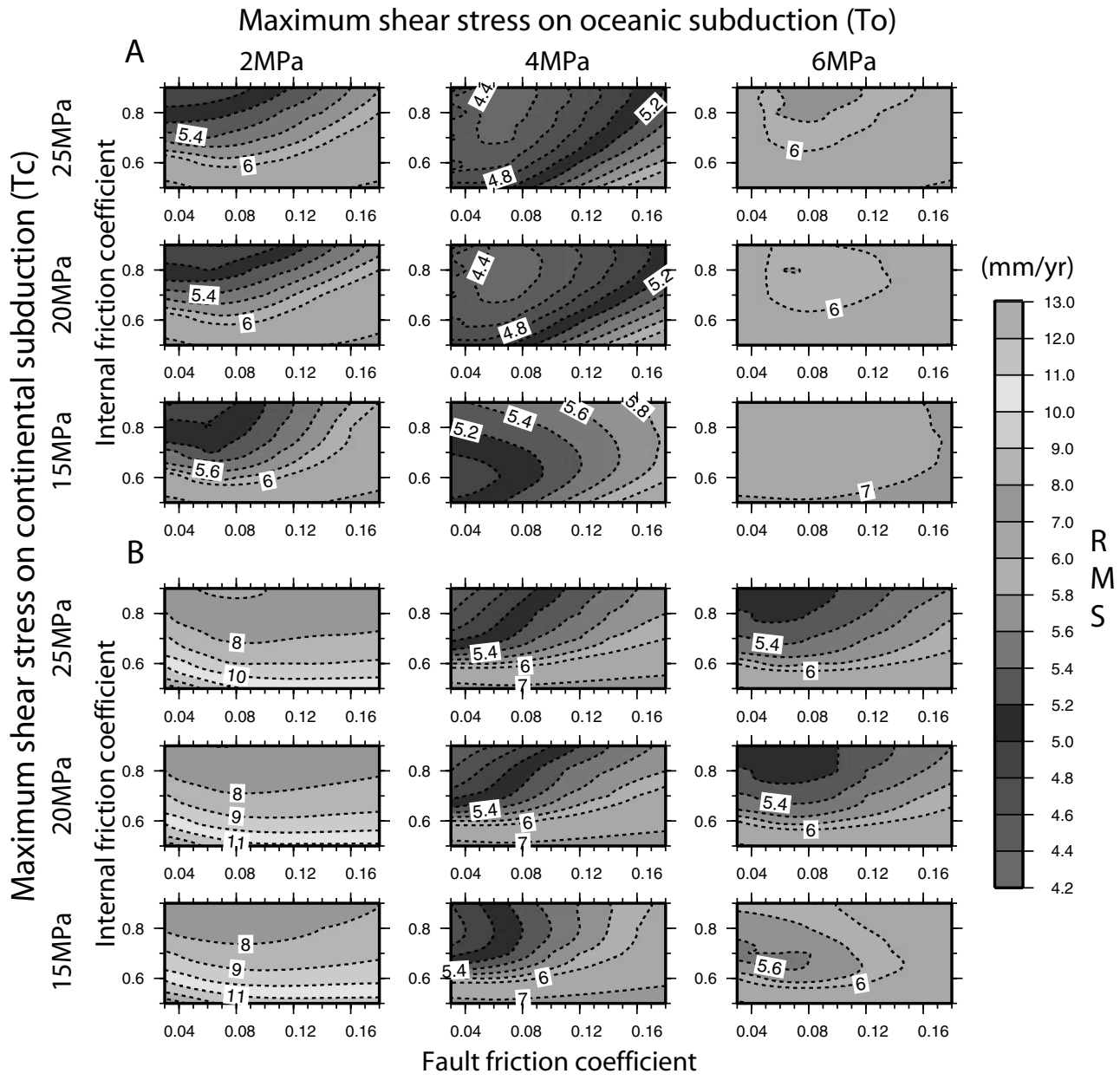

Figure 7. Result of the model parameter grid search for the (a) weaker and (b) stronger lithospheres tested here. Contour lines show the RMS of the fit of GPS (Figure 2) to model velocities.

Kong, 1994; *Bird*, 1998; *Kong and Bird*, 1996; *Jiménez-Munt et al.*, 2001; *Jiménez-Munt and Negredo*, 2003; *Liu and Bird*, 2002a] find fault friction coefficients (f_f) significantly smaller than internal friction, with values usually less than 0.2. We therefore tested fault friction coefficient in the 0.04–0.20 range.

[24] In an early deformation model of Asia, *Bird* [1978] used maximum shear traction on the Indian continental subduction (T_c) in the 20–30 MPa range, a value later amended to 15 MPa by *Kong and Bird* [1996] and *Lesne* [1999]. The same authors proposed a range of possible values for the maximum shear tractions at oceanic subductions (T_o). On the basis of these previous studies, we tested values ranging from 15 to 30 MPa for T_c and from 0.2 to 6 MPa for T_o.

4.2. Results

[25] The RMS misfit between modeled and observed velocities range from 4.2 to 16.8 mm a^{-1} (Figure 7). We find the smallest RMS for a maximum shear traction of 20 MPa or higher at continental subductions and 4 MPa or higher at oceanic subductions, regardless of the strong versus weak lithosphere tested here. The best fit value ranges from 0.7 to 0.9 for the internal friction coefficient and from 0.04 to 0.10 for the fault friction coefficient.

[26] The lowest RMS for the strong lithosphere case is 4.5 mm a^{-1}, slightly higher than that obtained with the weaker lithosphere (Figure 7). Moreover, the parameter search for the strong lithosphere case does not show a clear minimum within the bounds imposed in the search. Pre-

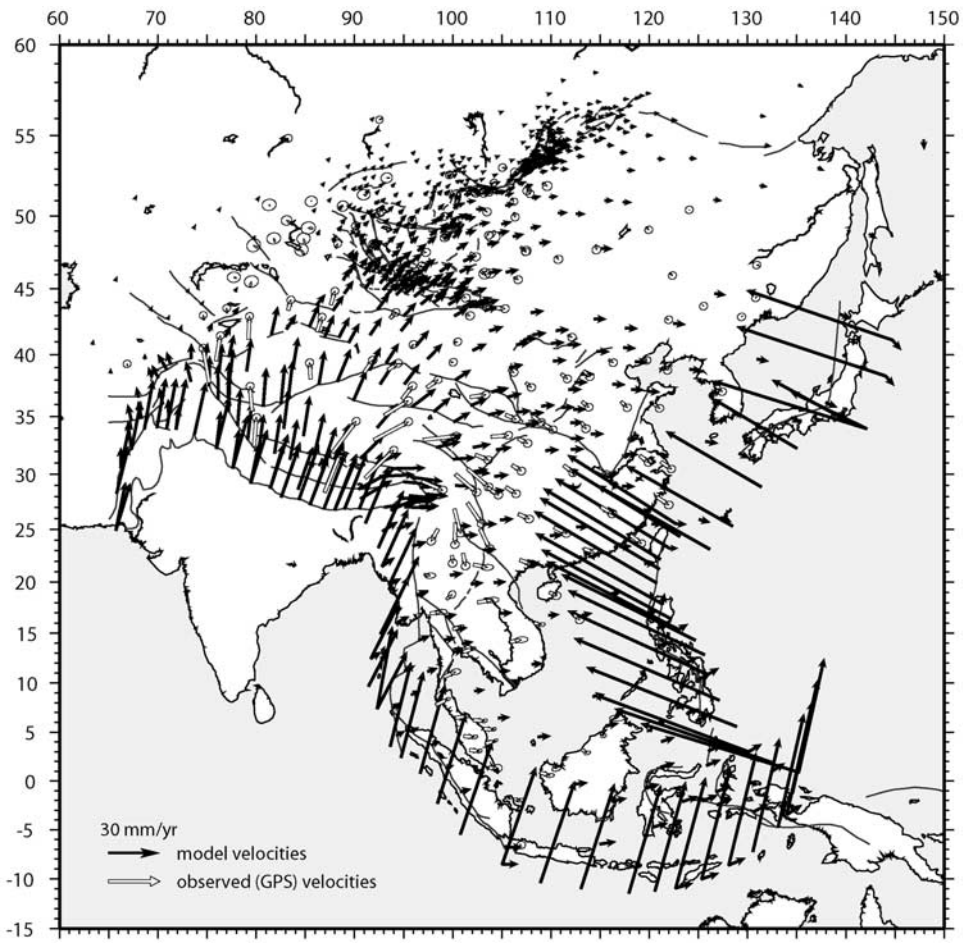

Figure 8a. Reference model, model (black arrows) and observed (white arrows) horizontal velocities. Choice of model parameters is explained in text (section 4.2) and summarized in Table 3.

dicted surface velocities using the best fit parameter set for the strong lithosphere case are significantly faster than for the weaker lithosphere, by 10 to 75% in Tibet, 100 to 180% in north China, Mongolia and Baikal, and 50 to 100% in east and south China. In southeast Asia, both models predict velocities in good agreement with observed GPS velocities.

[27] We find the best fit set of parameters (RMS = 4.2 mm a^{-1}) using the weaker lithosphere with $f_i = 0.8$, $f_f = 0.06$, $Tc =$ 20 MPa, and $To = 4$ MPa. Figures 8a (model and observed GPS velocities) and 8b (residual velocities) show predicted surface velocities derived from this set of parameters in good agreement with the observed ones, both in direction and magnitude, for Tibet, south China, Tien Shan, and Southeast Asia. Model extension rate across the Baikal rift zone is 1.5–3 mm a^{-1}, slightly lower than GPS observations. Observed velocity directions in the Altay, their clockwise rotation across the Gobi-Altay and central Mongolia, and the east to southeastward directions in north China are well reproduced. However, model velocities are overestimated in the Gobi desert (~9 mm a^{-1} against 4 mm a^{-1} observed), central Mongolia (6–7 mm a^{-1} against 3–4 mm a^{-1} observed) and north China (6–7 mm a^{-1} against 3–5 mm a^{-1} observed), and the model does not reproduce the rapid clockwise rotation observed around the eastern Himalayan syntaxis in the Yunnan. The model fit to the observed GPS velocities may possibly be improved by allowing for regional variations in interplate coupling and/or friction coefficients, which is beyond the scope of this study.

5. Testing the Force Balance

[28] In a second step, we seek to quantify the relative importance of (1) boundary forces resulting from the relative motion of neighboring plates and interplate coupling (using a maximum shear traction as a proxy for stress transfer at subductions), and (2) buoyancy forces resulting from GPE gradients. We use the thermal and constitutive parameters described above and run a series of experiments in which the contribution of GPE gradients and relative plate motions are progressively added to the models.

[29] In a first model (model 1, Table 3), we set the maximum shear traction at all convergent plate boundaries to zero (including the India/Eurasia boundary along the Himalayan front), thereby imposing free slip (or no mechanical coupling) between Asia and the adjacent plates. Boundary conditions along the northern and western sides of the model are fixed to zero displacement, as described above. Deformation in this model is therefore driven by buoyancy forces only. The resulting surface velocity field (Figure 9) shows very fast south directed velocities in the Himalayas and southern Tibet and fast southeast directed velocities in southeast Asia that obviously do not match

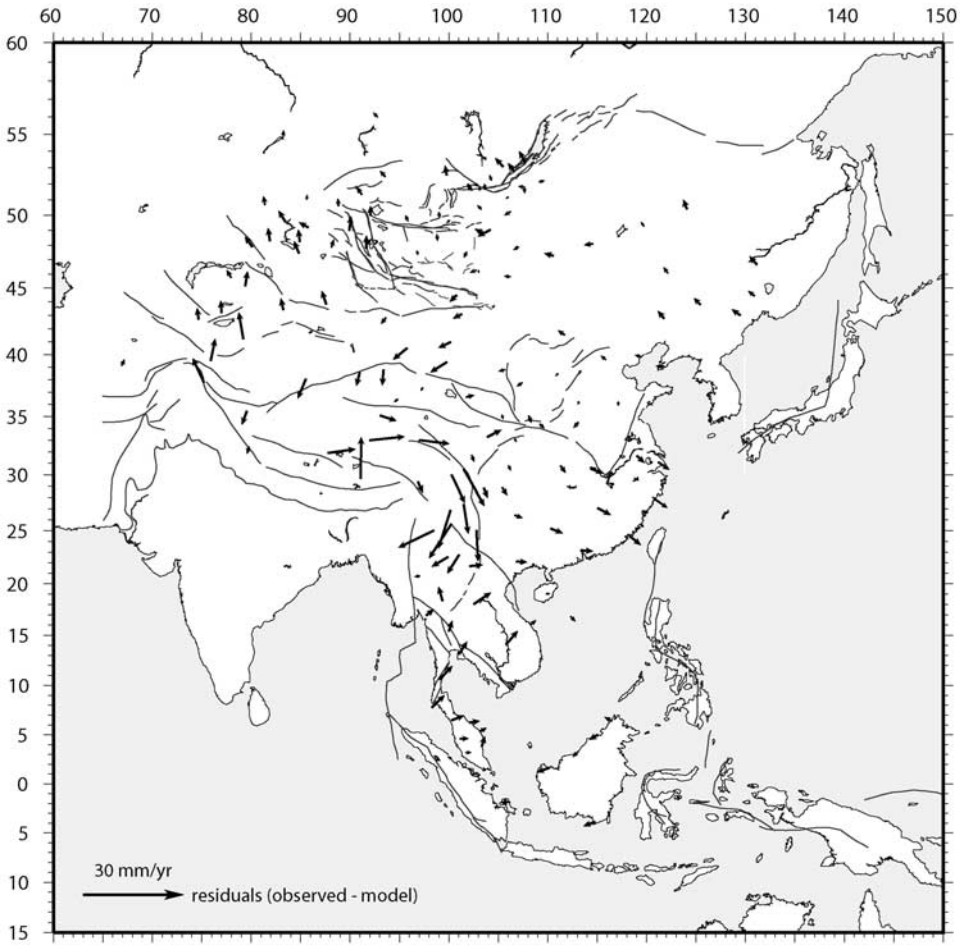

Figure 8b. Reference model, residuals (observed minus model) velocities. Note the difference in velocity scale with Figure 8a. Choice of model parameters is explained in text (section 4.2) and summarized in Table 3.

the observed GPS velocities in magnitude or direction. Shortening in the Tien Shan and the Mongolian Altay (western Mongolia) are not reproduced either. Predicted velocity magnitudes in the rest of the model are also overestimated, by about a factor of 5. Predicted extension across the Baikal rift zone is 10 mm a^{-1}, about 3 times faster than observed.

[30] This first experiment shows, as expected, that buoyancy forces alone are not sufficient to reproduce the major compressional structures of Asia (Himalayas, Tien Shan, Altay). The Himalayas and most of Tibet collapse southward in the absence of a resisting boundary force along the India/Eurasia continental subduction. This south directed collapse is a result of larger elevation differences (and therefore GPE gradients) along the southern border Tibet (India) than along its northern border with the Tarim basin and Mongolian plateau. In spite of the very large misfits, we note that this model driven by buoyancy forces only reproduces well the southeastward velocity directions observed in north China, central and eastern Mongolia, and south China, as well as the clockwise rotation observed in GPS velocities in the vicinity of the Gobi Altay.

[31] In a second set of experiments, we add the contribution of boundary forces. First, we establish a resisting force at the India/Eurasia and Arabia/Eurasia continental subductions by imposing a maximum shear traction of 20 MPa along these boundaries, the value found in the parameter search described above. We set the velocity of the Indian and Arabian plates to zero. As previously, we impose zero maximum shear traction at the oceanic subductions and keep the western and northern boundaries of the model confined

Table 3. Summary of Parameters Used in the Experiments Reported in Section 5[a]

				Boundary Velocities With Respect to Eurasia		
Experiments	Bathymetry	*Tc*, MPa	*To*, MPa	IN, Ar	AUS, Ph, PAC	NAM
1	actual	0	0	-	-	0
2	actual	20	0	0	-	0
3	actual	20	0	REVEL	-	0
4	actual	20	4	REVEL	0	FREE
5	modified	20	4	REVEL	REVEL	REVEL
REF	actual	20	4	REVEL	REVEL	REVEL

[a]REF, reference model, section 4.2. For all described experiments, internal friction coefficient is 0.8 and fault friction coefficient is 0.06. Plates are EU, Eurasia; IN, India; Ar, Arabia; AUS, Australia; Ph, Philippines Sea; PAC, Pacific; NAM, North America.

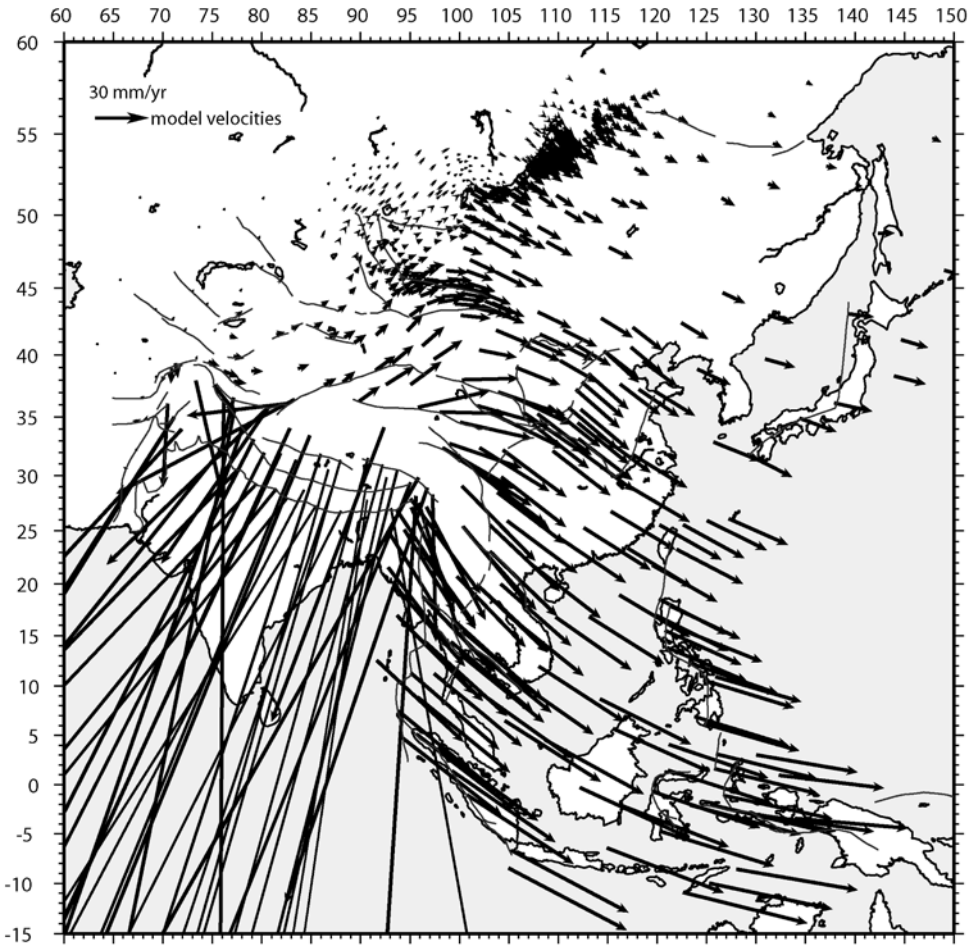

Figure 9. Model 1, horizontal surface velocities predicted by a model involving only gravitational potential energy gradients. See Table 3 and text (section 5) for a full explanation of the model parameters.

(model 2, Table 3). The resulting model velocities (Figure 10) are close to zero in the Himalayas and southern Tibet, as the collapse of these structures found in the previous models is now resisted by the strength of the India/Eurasia plate contact. Model velocities show shortening along the northern edge of Tibet, in the Tien Shan, and in the Altay and Gobi Altay mountains, but at slower rates than observed. In the rest of Asia, the velocity pattern is similar to the first model described above, but generally larger (by a factor of 2 to 3 from northwest Tibet to the Siberian platform, 1.2 in eastern Mongolia, Baikal and north China, 1.2 to 1.4 in southeast Asia). Velocities in south China remain unchanged.

[32] This experiment illustrates how coupling at the India/Eurasia plate boundary balances the effect of buoyancy forces in Tibet and allows for compressional stresses to be transferred into Asia. Interestingly, India-Eurasia convergence is not necessary to reproduce the observed eastward and southeastward motions in most of north and east Asia, provided that appropriate buoyancy forces are acting along the eastern and southeastern sides of the model.

[33] Second, we apply the India/Eurasia relative plate velocity at the India/Eurasia plate boundary along the Himalayan front, and the Arabia/Eurasia relative plate velocity at the Arabia/Eurasia plate boundary. All other parameters are kept similar to the previous experiment (model 3, Table 3). Model velocities (Figure 11) are now close to the observed ones in the Himalayas and southern Tibet and show shortening in the Tien Shan and Altay mountains at a rate close to the GPS observations. Model velocities are overall larger than in the previous model, by a factor of 2 in the western half of Asia, 1.5 in Tibet, Mongolia, Baikal, and north China and 1.2 in south China and southeast Asia. Plate convergence and high mechanical coupling between India and Eurasia therefore allow us to reproduce the compressional strain observed in the Himalayas, Tien Shan, and Mongolia Altay. However, velocities in most of north and east Asia are overestimated (up to 10 times in northern Asia), velocities in Yunnan do not show the observed clockwise rotation around the eastern Himalayan syntaxis, and velocities in southeast Asia are not well reproduced.

[34] Third, we establish a resisting force at the oceanic subductions in east and southeast Asia by imposing a maximum shear traction of 4 MPa, the value found in the parameter search described above. We impose velocities of the Australian, Philippines and Pacific plates to be zero in all direction along their boundary with Eurasia. All other model parameters are kept similar to the previous case (model 4, Table 3). Compared to the previous experiment,

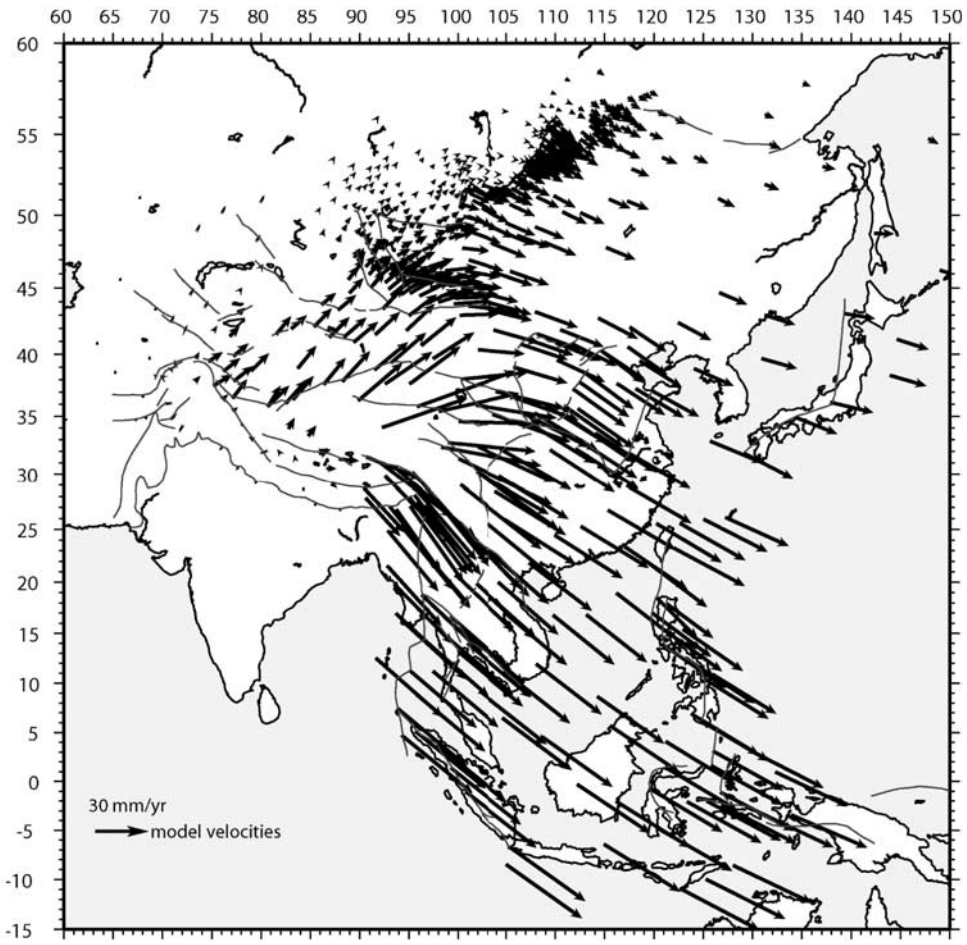

Figure 10. Model 2, horizontal surface velocities predicted by a model involving gravitational potential energy gradients, a 20 MPa maximum shear traction at continental subductions, and zero velocity along the continental-Eurasia plate boundaries. See Table 3 and text (section 5) for a full explanation of the model parameters.

model velocities (Figure 12) decrease significantly over the entire domain, as expected from adding a resisting force along the eastern border of the model, in particular in southeast Asia where they drop from 50–55 mm a^{-1} to 0–5 mm a^{-1}. In the rest of Asia, velocities decrease by a factor of 6 (south China) to 1.2 (Tibet) but remain significantly faster than observed. Model velocities are now directed eastward to east-northeastward, instead of southeastward as found in the previous experiments or in the GPS data.

[35] Finally, we restore actual relative plate motions along the oceanic subductions in east and southeast Asia, and between North America and Eurasia at the northeastern edge of the model. All other parameters are kept similar to the previous case. This experiment therefore uses the same parameters as the best fit model described in section 4.2 (Figures 8a and 8b; model REF, Table 3). Compared to the previous experiment, model velocities decrease over most of Asia (by a factor of 1.2 to 1.5 in the Tien Shan and south China, and 1.5 to 2 in Mongolia-Baikal and north China) to reach magnitudes that are now consistent with the observations. Model velocity directions are, however, systematically rotated counterclockwise by 10–15° compared to the observations in north and south China. The fit is, however, very good in southeast Asia, both in magnitude and direction, although the observed clockwise rotation around the eastern Himalayan syntaxis is still not reproduced.

6. Discussion

6.1. Role of Buoyancy Forces

[36] This series of experiments illustrates the interplay between buoyancy and boundary forces in driving present-day deformation in Asia. We find that buoyancy forces are significant overall and may drive, for a large part, the east to southeastward motions observed in south and north China and in central Mongolia. In our experiments, these buoyancy forces need to be resisted by compressional boundary forces along the oceanic subductions that bound Asia to the east and southeast in order to match the observed velocities. These resisting boundary forces result from the convergence of adjacent oceanic plates toward Eurasia and interplate coupling at the oceanic subductions. However, buoyancy forces alone do not explain present-day deformation in most of the western half of the domain, where N-S shortening dominates (Himalayas, Tibet, Tien Shan, Altay). Deformation in these areas is well reproduced with strong coupling

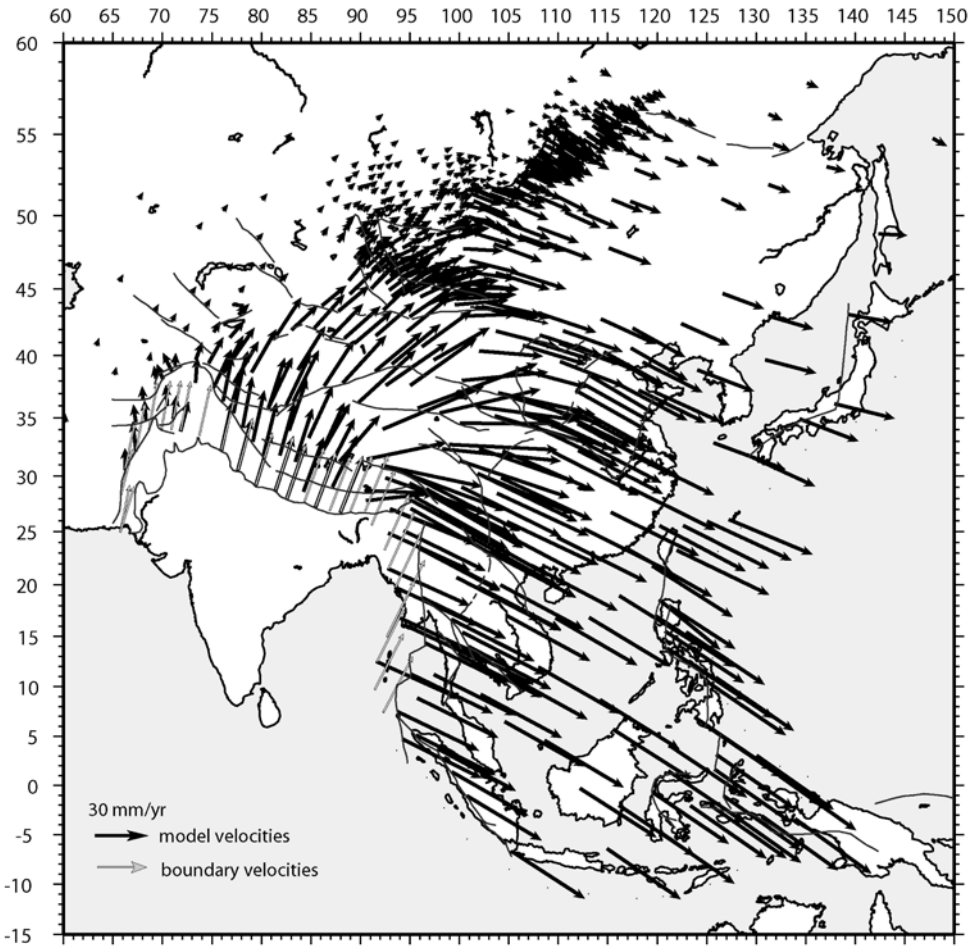

Figure 11. Model 3, horizontal surface velocities predicted by a model involving gravitational potential energy gradients, a 20 MPa maximum shear traction at continental subductions, and REVEL velocities [*Sella et al.*, 2002] along the continental-Eurasia plate boundaries. See Table 3 and text (section 5) for a full explanation of the model parameters.

at the India/Eurasia plate contact, that allows for compressional boundary stresses to transfer into Asia.

[37] *Flesch et al.* [2001] also underlined the importance of buoyancy forces in driving deformation in Asia. In their models, buoyancy forces result only from GPE gradients across continental Asia. In order to further investigate the origin of the buoyancy forces acting in our models, we show an additional experiment where we set the bathymetry and heat flow in oceanic domains to -100 m and 55 mW m^{-2}, respectively, thereby removing GPE gradients, and the resulting buoyancy forces, across oceanic margins. All other parameters are kept identical to the reference experiment (model 5, Table 3). We find that model velocities are similar to the reference model in the western half of Asia, whereas eastward motions in south and north China and SE Asia are not reproduced anymore (Figure 13). We conclude that the eastward motions obtained in our reference model in eastern Asia are mostly driven by buoyancy forces originating at the eastern and southeastern oceanic margins of Asia, where GPE gradients generate oceanward tensional stresses that tend to pull east and southeast Asia toward the subductions.

[38] This may, however, be an oversimplification of the process actually at work, since our models do not simulate the actual dynamics of subduction zones. For instance, we do not account for slab pull or for corner flow between the upper plate lithosphere and the subducting slab. Also, the maximum shear stress imposed at subductions in the models is a simple proxy for stress transfer rather than a true physical representation of mechanical coupling. However, it remains that the eastward and southeastward motions observed in north China, south China, and SE Asia are reproduced only if tensional, oceanward stresses are applied to the southeastern and eastern boundaries of the domain.

6.2. Could Boundary Forces Suffice?

[39] In one of the first experiments on the dynamics of deformation in Asia, *Peltzer and Tapponnier* [1988] successfully reproduced some of the geological observables in Asia, using India-Eurasia collision as the only driving force, while the eastern and southeastern boundaries of the model were left unconfined. *Peltzer and Saucier* [1996] further quantified this result numerically assuming an elastic, faulted, lithosphere and, again, India-Eurasia collision as the only driving force. Both models predict that strike-slip faults in Asia slip at fast rates, up to 20–30 mm a^{-1} for the Altyn Tagh fault. Here, we test whether a model driven by

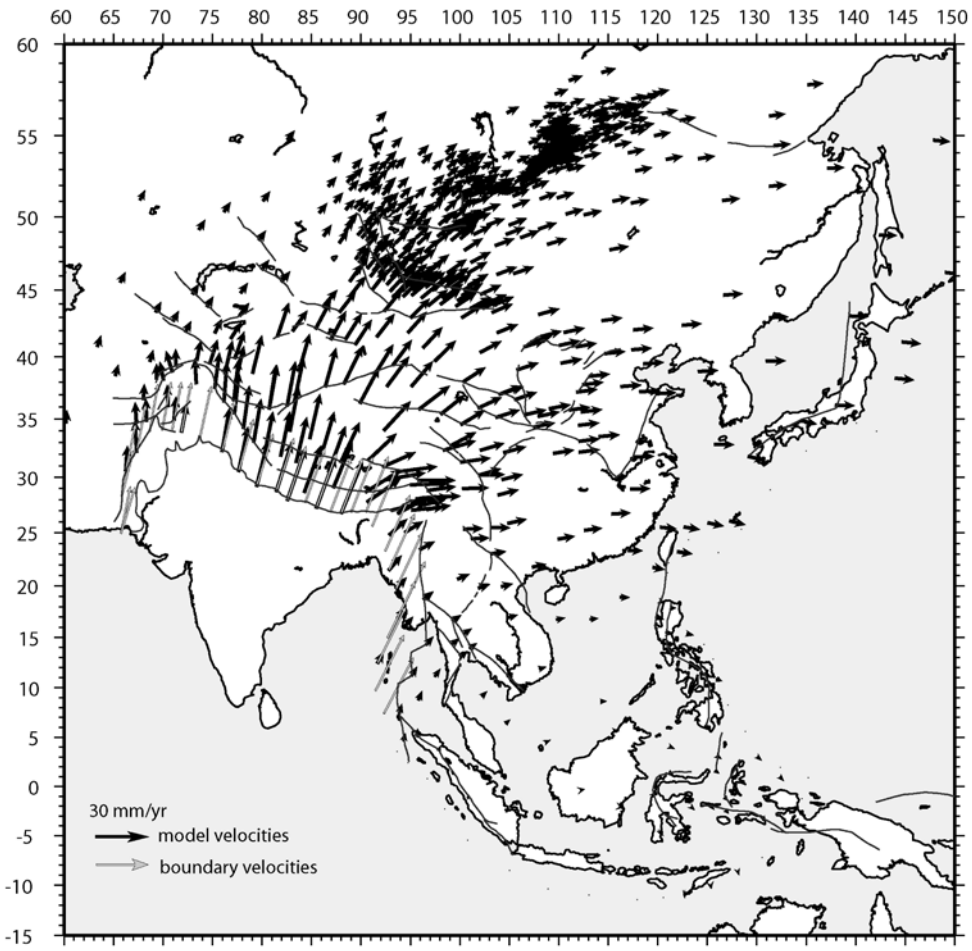

Figure 12. Model 4, horizontal surface velocities predicted by a model involving gravitational potential energy gradients, a 20 MPa maximum shear traction at continental subductions, a 4 MPa maximum shear traction at the oceanic subduction, and the REVEL velocities [*Sella et al.*, 2002] along the continental-Eurasia plate boundaries. See Table 3 and text (section 5) for a full explanation of the model parameters.

India-Eurasia collision alone can explain the GPS current observations.

[40] To simulate experimental conditions as close as possible to these early edge-driven models, we cancel the effect of buoyancy forces by setting constant elevation (910 m) and heat flow (65 mW m^{-2}) over the entire model. To simulate an unconfined eastern boundary, we treat the southeast and east Asia subductions as free displacement boundaries, allowing slip in any direction. We decrease the fault friction coefficient to 0.01 to enhance slip on faults. To simulate the indenting mechanism of India, we treat the India-Eurasia collision as a displacement fixed boundary and impose the reference model velocities along the Himalayan frontal thrust as boundary conditions. Boundary conditions along the northern and western sides of the model are kept the same as the reference model (section 3.2). Figure 14 shows that this experimental setup results in horizontal velocities that are in fair agreement with the observed ones, with an RMS misfit of 4.7 mm a^{-1}. We also find that model velocities are similar to those obtained in the reference model (Figure 8a) and to those predicted by *Peltzer and Saucier* [1996]. Predicted fault slip rates in this experiment are higher than in the reference model for the Karakorum and Altyn Tagh faults, the two fastest slipping faults in the *Peltzer and Saucier* [1996] model, but do not exceed 8 mm a^{-1} (see section 6.4). Slip rates on other faults are lower than in the reference model and than the observed Quaternary rates (see section 6.4). Shortening across the Himalayas, Tien Shan, and Altay is also twice as small as the GPS observations or the reference model. Predicted extension across the Baikal rift zone is also smaller than observed (0.5–1.5 mm a^{-1} against 3–4 mm a^{-1}) and model velocities on the Khazak and Siberian platforms (4–7 mm a^{-1}) differ significantly from the observations or the reference model (0–3 mm a^{-1}).

[41] In spite of these differences, one may argue that a model in which the deformation in Asia is forced only by a velocity condition applied at the boundary between India and Eurasia provides a reasonable fit to current GPS data. This, however, assumes that buoyancy forces in and around Asia and boundary forces along the Indonesian and Pacific subductions have a negligible contribution to the force balance. Our experiment, as well as other dynamic models [e.g., *England and Molnar*, 1997a; *Flesch et al.*, 2001; *England and Molnar*, 2005], however, show that GPE gradients in Asia generate buoyancy forces comparable to

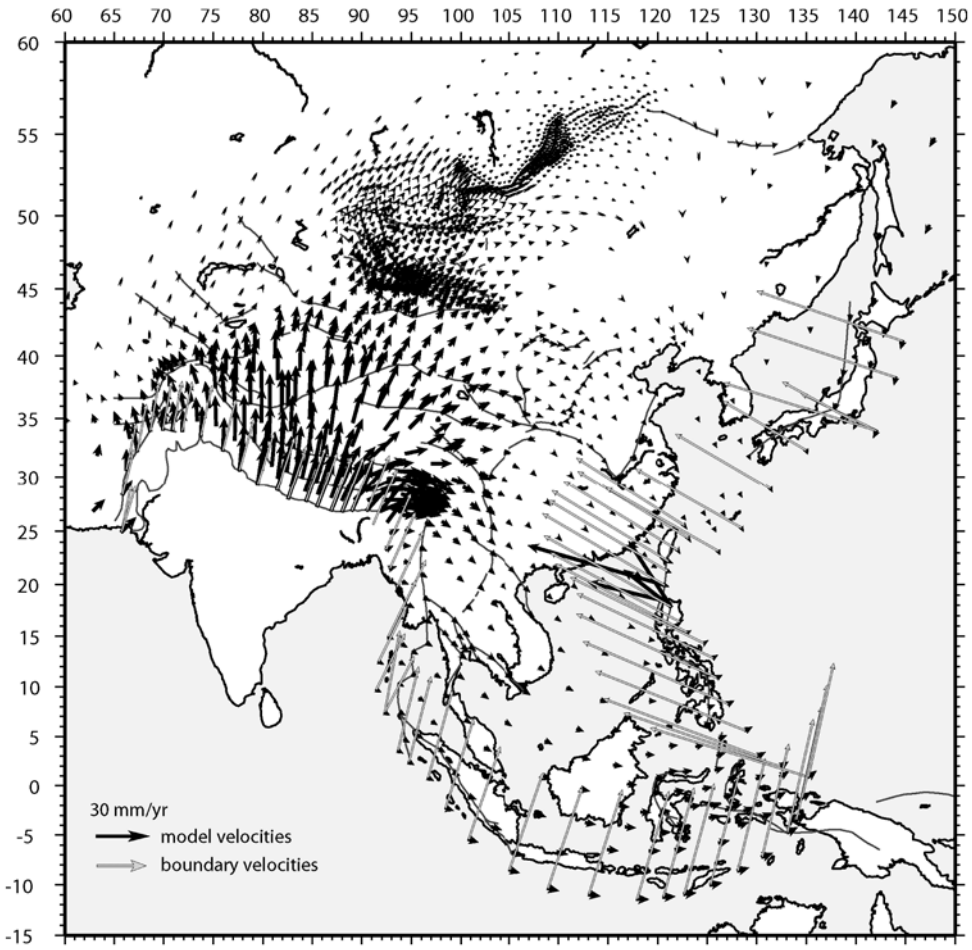

Figure 13. Model 5, horizontal surface velocities predicted by a model involving boundary and buoyancy forces as in the reference model except that the buoyancy forces result only from gravitational potential energy gradients in the continents. See Table 3 and text (section 6.1) for a full explanation of the model parameters.

boundary forces in their effect on surface deformation. Also, large earthquakes at oceanic subductions in east and southeast Asia require some degree of interplate coupling, inconsistent with the free boundary assumption used in the model above. The model setup used here is therefore likely to be missing some first-order geophysical processes. We thus do not favor an interpretation of the dynamics of the deformation based on boundary forces alone.

6.3. Pervasive Versus Localized Strain

[42] The question of the forces driving continental deformation in Asia is typically merged to that of strain distribution, with edge-driven models arguing for localized strain on faults, while thin sheet models argue for continuous deformation. Since the approach used here allows for slip on faults and lateral variations of lithospheric strength, it is useful to investigate the spatial distribution of strain in our best fit model, recalling that it includes both boundary stresses and buoyancy stresses.

[43] Figure 15 shows that model strain rates are not significant (i.e., less than 3×10^{-9} a^{-1}, the average precision of the GPS measurements used here) over a very large part of Asia (most of north China, south China, and Sunda). They are significant in the Himalayas, central and eastern Tibet, the Pamir-Tien Shan and Altay ranges, western Mongolia, and the Baikal rift zone. This result matches well the spatial distribution of strain rates derived directly from GPS observations [*Calais et al.*, 2006]. It is also consistent with denser GPS measurements in Tibet [*Chen et al.*, 2004], which show that about 50% of the observed velocity field is explained by distributed deformation across the Tibetan Plateau, the Qaidam basin, and the Qilian Shan, while the remaining 50% is accommodated by slip on a limited number of faults. The same GPS measurements show a combination of east-west extension and north-south compression in Tibet, which is well reproduced in our best fit model (Figure 15).

[44] From the best fit model results, validated against the GPS observations, we calculate the effective lithospheric viscosity as the vertically averaged stress over strain rate. The map of effective viscosity (Figure 16) shows lateral variations from 3×10^{21} to 7×10^{22} Pa s in Tibet and other high-elevation areas, to $\sim 10^{24}$ Pa s in low-elevation and cratonic areas. These effective viscosity estimations are consistent with previous results from *Flesch et al.* [2001], who also find lateral variations of vertically averaged

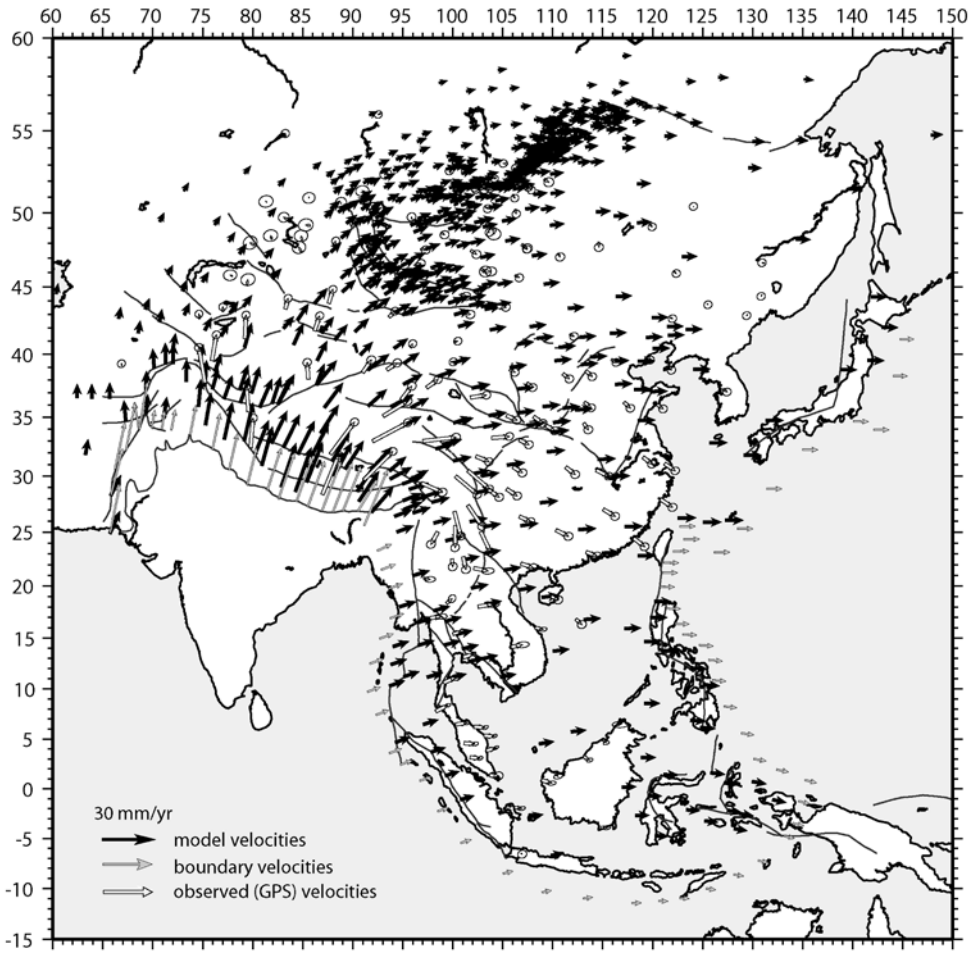

Figure 14. Model 6, horizontal surface velocities predicted by a model involving no gravitational potential energy gradients, and simulating free motion at oceanic subductions and the India-Eurasia relative plate velocities at the India-Eurasia plate boundary. See text (section 6.2) for a full explanation of the model parameters.

effective viscosity by up to 3 orders of magnitude between Tibet and its surroundings.

6.4. Fault Slip Rates

[45] In addition to surface velocities, we calculate model slip rates on major active faults, that we compare to Holocene estimates from geologic data [e.g., *Lasserre et al.*, 1999; *Van Der Woerd et al.*, 2000; *Tapponnier et al.*, 2001; *Brown et al.*, 2002; *Mériaux et al.*, 2004, 2005; *Chevalier et al.*, 2004; *Ritz et al.*, 1995, 2003; *Prentice et al.*, 2002; *San'kov et al.*, 2002] and to present-day estimates from geodetic data [*Bendick et al.*, 2000; *Chen et al.*, 2000; *Shen et al.*, 2001; *Wright et al.*, 2004; *Jade et al.*, 2004; *Wallace et al.*, 2004] (Figure 17). We find that the predicted sense of motion on all faults matches geologic observations. Model slip rates match Holocene and geodetic rates well in the Baikal rift zone [*San'kov et al.*, 2002], the Gobi Altay [*Ritz et al.*, 1995, 2003; *Prentice et al.*, 2002], and the Tien Shan [*Avouac*, 1991; *Molnar and Deng*, 1984; *Abdrakhmatov et al.*, 1996]. For all other faults, model slip rates are significantly smaller than Holocene rates but consistent with geodetic rates within errors (although typically at the lower edge of the geodetic error bar) for the Kunlun [*Chen et al.*, 2000], Central Altyn Tagh [*Bendick et al.*, 2000; *Shen et al.*, 2001; *Wallace et al.*, 2004], Haiyuan [*Lasserre et al.*, 1999], and Karakorum [*Van Der Woerd et al.*, 2000; *Brown et al.*, 2002; *Chevalier et al.*, 2004; *Wright et al.*, 2004] faults.

[46] We tested whether decreasing the fault friction coefficient would lead to a better match between observed and model fault slip rates. Since fault friction applies to all faults in the model, and since India-Eurasia interplate coupling and convergence are not sufficient to overcome buoyancy forces in Tibet with a low friction coefficient on the Himalayan frontal thrust, we treated the India-Eurasia collision as a displacement-fixed boundary, imposing the reference model velocities along that boundary of the model. All other model parameters and boundary conditions are kept identical to the best fit model presented above. A model with a fault friction coefficient of 0.01 leads to an RMS misfit of the predicted surface velocities of 5.2 mm a^{-1}, 1 mm a^{-1} larger than the best fit model described above. Model slip rates are larger than observed Holocene rates for faults where the reference model showed a good agreement (Gobi Altay, Baikal, Tien Shan), but match observed Holocene rates better for the Jiali and Kunlun faults (Figure 17). They are, however, still

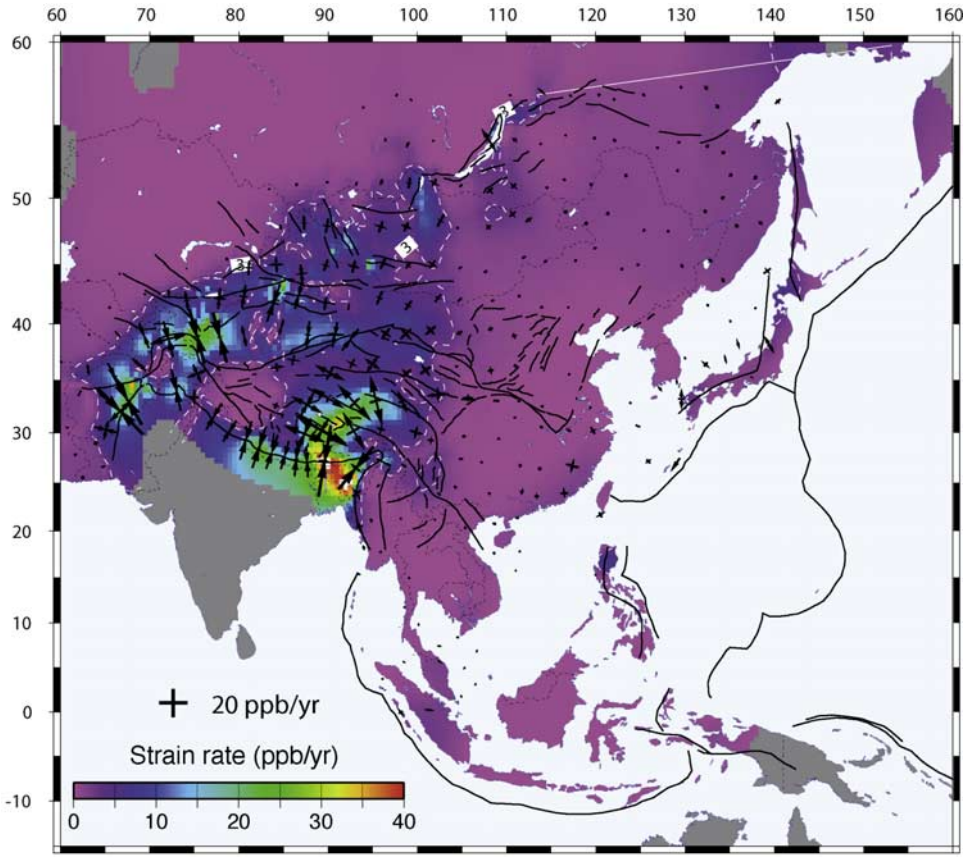

Figure 15. Second invariant of the strain rate tensor from the best fit model (color background). See section 4.2 and Table 3 for full explanation of the model parameters and Figures 8a and 8b for the representation of the best fit horizontal velocity field. The 3 ppb a^{-1} value is contoured for reference. Black crosses show principal strain rate directions. Convergent arrows indicate compression; divergent arrows indicate extension.

significantly slower than observed Holocene rates for the Altyn Tagh, Xianshuihe, and Karakorum faults.

[47] The disagreement between geodetic and Holocene fault slip rates in Asia is highly debated, with estimates that vary by a factor of two to five for the Altyn Tagh and Karakorum faults, for instance [e.g., *Mériaux et al.*, 2004; *Wright et al.*, 2004]. *England and Molnar* [2005] proposed that Holocene slip rates may be biased by an systematic underestimation of terrace riser ages. However, a recent radar interferometry study across the central part of the Altyn Tagh found a slip rate of 18 mm a^{-1} [*Socquet et al.*, 2005], in agreement with some Holocene estimates. Although the debate remains open, the dynamic models shown here require rates of 5 to 10 mm a^{-1} on the Altyn Tagh fault and are not consistent, overall, with the high slip rate values found by some Quaternary geology studies.

7. Conclusions

[48] We have shown that GPS-derived velocities in Asia and, to some extent, Holocene fault slip rates, can be explained by a balance of boundary and buoyancy forces acting on a faulted lithosphere with laterally varying strength. Model and observed strain rates match well. Both show no resolvable strain rates over most low-elevation regions, which also correspond to areas of high lithospheric strength (>10^{23} Pa s). Significant internal strain, possibly continuous, is limited to high-elevation areas, mechanically weaker (10^{21} to 10^{23} Pa s). Even though block- or plate-like motions provide an accurate kinematic description of surface deformation for a large part of Asia [*Calais et al.*, 2006], current GPS strain rates are consistent with the thin sheet physical framework [*England and Houseman*, 1986], with lateral variations of lithospheric strength controlling the style of deformation.

[49] GPS observations are consistent with a model in which subduction boundaries along the eastern and southern borders of Asia (Pacific, Philippines, and Australian plates) play a significant role in the dynamics of deformation in Asia [e.g., *Kong and Bird*, 1996]. Our experiments show that south China, north China, and Sunda are "pulled" eastward as a result of tensional, oceanward stresses rather than "extruded" as a result of India-Eurasia collision. These tensional stresses may result from GPE gradients across the active margins of eastern and southeastern Asia (as proposed here), or from other subduction processes not accounted for in our models (e.g., slab pull, corner flow). They may also result from viscous coupling between mantle flow and the base of the lithosphere ("basal drag"), a process absent from our models, but that may significantly

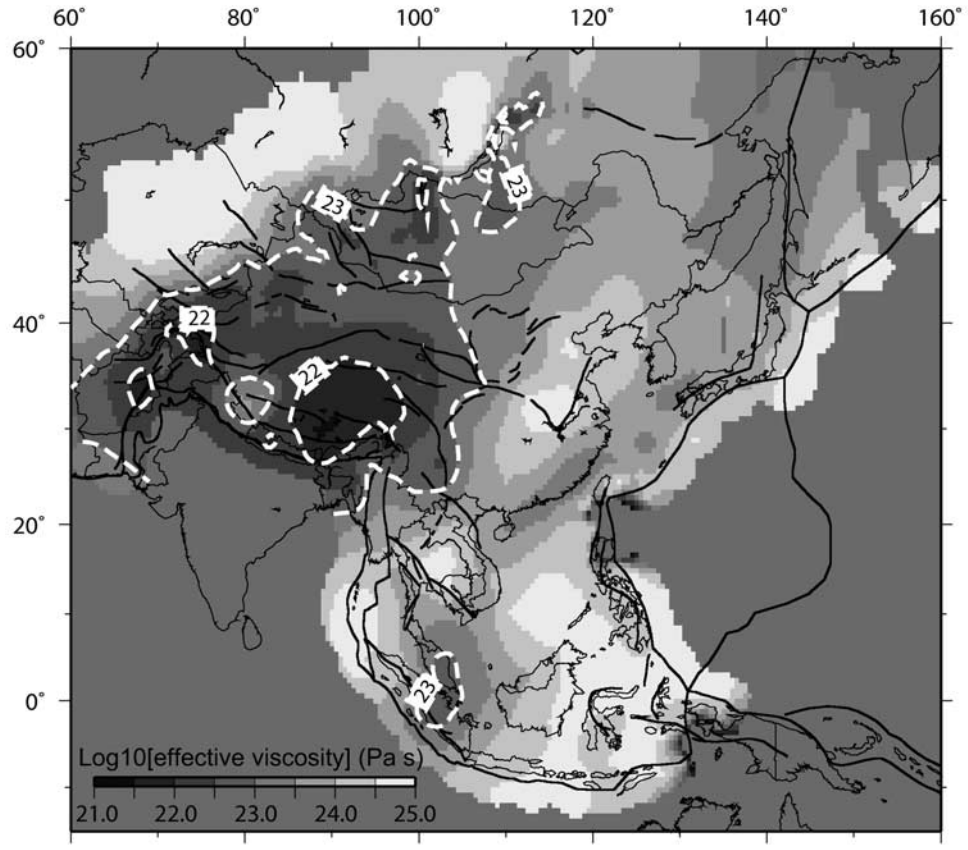

Figure 16. Vertically averaged effective viscosity (color background) (in Pa s) in the reference model. The amplitude is presented on a logarithmic scale. The 10^{22} and 10^{23} Pa s values are contoured for reference with white dashed lines.

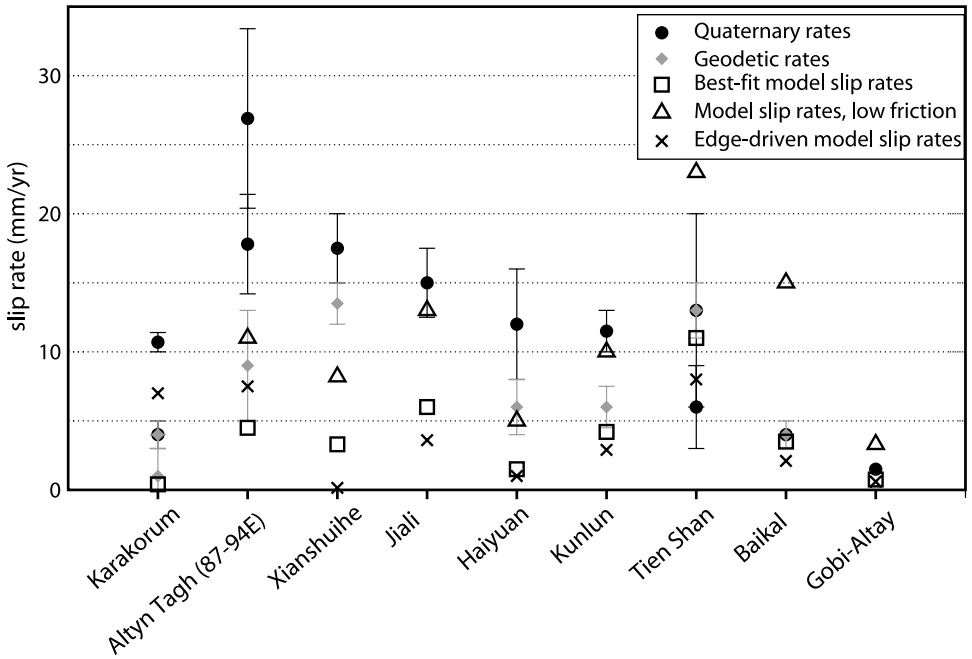

Figure 17. Comparison between Quaternary, geodetic, and model slip rates for major active faults in Asia. Best fit model (section 4.2) uses a fault friction coefficient of 0.06; low friction model (section 6.4) and edge-driven model (section 6.2) use a fault friction coefficient of 0.01. References for Quaternary and geodetic rates are given in the text.

contribute to the deformation of continents [*Bird*, 1998; *Becker and O'Connell*, 2000; *Bokelmann*, 2002].

[50] **Acknowledgments.** We thank Peter Bird for sharing his finite element code SHELLS and for his support and advice. This works follows preliminary unpublished results obtained by Olivia Lesne. We thank Jean Virieux, Carole Petit, and Andy Freed for their help using the code, and Jacques Déverchère and Lucy Flesch for insightful discussions on the tectonics of Asia. We gratefully acknowledge the constructive reviews of P.C. England and P. Tregoning that significantly helped improve the original manuscript. This research was supported by INSU-CNRS (''Intérieur de la Terre'' program) and NSF award EAR-0609337. UMR Géosciences Azur, CNRS-UNSA contribution.

References

Abdrakhmatov, K., et al. (1996), Relatively recent construction of the Tien-Shan inferred from GPS measurements of present-day crustal deformation rates, *Nature*, *384*, 450–453.

Agar, S. M., and K. D. Klitgord (1995), Rift flank segmentation, basin initiation and propagation: A neo-tectonic example from lake Baikal, *J. Geol. Soc. London*, *152*, 849–860.

Argus, D., and M. Heflin (1995), Plate motion and crustal deformation estimated with geodetic data from the Global Positioning System, *Geophys. Res. Lett.*, *22*, 1973–1976.

Artemieva, I. M., and W. D. Mooney (2001), Thermal thickness and evolution of Precambrian lithosphere: A global study, *J. Geophys. Res.*, *106*, 16,387–16,414.

Avouac, J. P. (1991), Application des méthodes de morphologie quantitative à la néotectonique, Modèle cinématique des déformations actives en Asie Centrale, Ph.D. thesis, Univ. Denis Diderot-Paris 7, Paris.

Avouac, J. P., and P. Tapponnier (1993), Kinematic model of active deformation in central Asia, *Geophys. Res. Lett.*, *20*, 895–898.

Baljinnyam, I., et al. (1993), Ruptures of major earthquakes and active deformation in Mongolia and its surroundings, *Mem. Geol. Soc. Am.*, *181*, 62 pp.

Becker, T., and R. O'Connell (2000), On the driving forces of plate tectonics, *Eos Trans. AGU*, *81*(48), Fall Meet. Suppl., Abstract U72A-02.

Bendick, R., R. Bilham, J. Freymueller, K. Larson, and G. Yin (2000), Geodetic evidence for a low slip rate in the Altyn Tagh fault system, *Nature*, *404*, 69–72.

Bilham, R., K. Larson, and J. Freymueller (1997), GPS measurements of present-day convergence across the Nepal Himalaya, *Nature*, *386*, 61–64.

Bird, P. (1978), Initiation of intracontinental subduction in the Himalaya, *J. Geophys. Res.*, *83*, 4975–4987.

Bird, P. (1989), New finite element technique for modeling deformation histories of continents with stratified temperature-dependent rheology, *J. Geophys. Res.*, *94*, 3967–3990.

Bird, P. (1996), Computer simulations of Alaskan neotectonics, *Tectonics*, *15*, 235–236.

Bird, P. (1998), Testing hypotheses on plate-driving mechanisms with global lithosphere models including topography, thermal structure and faults, *J. Geophys. Res.*, *103*, 10,115–10,129.

Bird, P. (1999), Thin-plate and thin-shell finite-element programs for forward dynamic modeling of plate deformation and faulting, *Comput. Geosci.*, *25*, 383–394.

Bird, P., and J. Baumgardner (1984), Fault friction, regional stress, and crust-mantle coupling in southern California from finite element models, *J. Geophys. Res.*, *89*, 1932–1944.

Bird, P., and X. Kong (1994), Computer simulations of California tectonics confirm very low strength of major faults, *Geol. Soc. Am. Bull.*, *106*(2), 159–174.

Bock, Y., L. Prawirodirdjo, J. F. Genrich, C. W. Stevens, R. McCaffrey, C. Subarya, S. S. O. Puntodewo, and E. Calais (2003), Crustal motion in Indonesia from Global Positioning System measurements, *J. Geophys. Res.*, *108*(B8), 2367, doi:10.1029/2001JB000324.

Bokelmann, G. (2002), Convection-driven motion of the North American craton: Evidence from P-wave anisotropy, *Geophys. J. Int.*, *148*, 278–287.

Bourtchevskaia, M., R. Mellors, E. Calais, and V. Sankov (2005), A source model for the 2003 Altai earthquake from InSAR and GPS data, *Eos Trans. AGU*, *86*(52), Fall Meet. Suppl., Abstract G51C-0837.

Brace, W. F., and D. L. Kohlstedt (1980), Limits on lithospheric stress imposed by laboratory experiments, *J. Geophys. Res.*, *85*, 6248–6252.

Brown, E. T., R. Bendick, D. L. Bourlès, V. Gaur, P. Molnar, G. M. Raisbeck, and F. Yiou (2002), Slip rates of the Karakorum fault, Ladakh, India, determined using cosmic ray exposure dating of debris flows and moraines, *J. Geophys. Res.*, *107*(B9), 2192, doi:10.1029/2000JB000100.

Burchfiel, B. C., and L. H. Royden (1991), Tectonics of Asia 50 years after the death of Emile Argand, *Eclogae Geol. Helv.*, *84*, 599–629.

Byerlee, J. D. (1978), Friction of rocks, *Pure Appl. Geophys.*, *116*, 615–626.

Calais, E., and S. Amarjargal (2000), New constraints on current deformation in Asia from continuous GPS measurements at Ulan Baatar, Mongolia, *Geophys. Res. Lett.*, *27*, 1527–1530.

Calais, E., O. Lesne, J. Déverchère, V. Sankov, A. Lukhnev, A. Miroshnitchenko, V. Buddo, K. Levi, V. Zalutzky, and Y. Bashkuev (1998), Crustal deformation in the Baikal rift from GPS measurements, *Geophys. Res. Lett.*, *25*(21), 4003–4006.

Calais, E., M. Vergnolle, V. San'kov, A. Lukhnev, A. Miroshnitchenko, S. Amarjargal, and J. Déverchère (2003), GPS measurements of crustal deformation in the Baikal-Mongolia area (1994–2002): Implications for current kinematics of Asia, *J. Geophys. Res.*, *108*(B10), 2501, doi:10.1029/2002JB002373.

Calais, E., L. Dong, M. Wang, Z. Shen, and M. Vergnolle (2006), Continental deformation in Asia from a combined GPS solution, *Geophys. Res. Lett.*, *33*, L24319, doi:10.1029/2006GL028433.

Cattin, R. (1997), Modélisation du cycle sismique en zone de subduction, application à la région du Nord Chili, Ph.D. thesis, Univ. Denis Diderot-Paris 7, Paris.

Cattin, R., H. Lyon-Caen, and J. Chéry (1997), Quantification of intraplate coupling in subduction zones and forearc topography, *Geophys. Res. Lett.*, *24*, 1563–1566.

Chen, Q., J. T. Freymueller, Q. Wang, Z. Yang, C. Xu, and J. Liu (2004), A deforming block model for the present-day tectonics of Tibet, *J. Geophys. Res.*, *109*, B01403, doi:10.1029/2002JB002151.

Chen, W. P., and P. Molnar (1983), Focal depths of intracontinental and intraplate earthquakes and their implications for the thermal and mechanical properties of the lithosphere, *J. Geophys. Res.*, *88*, 4183–4214.

Chen, Z., B. C. Burchfiel, Y. Liu, R. W. King, L. H. Royden, W. Tang, E. Wang, J. Zhao, and X. Zhang (2000), Global Positioning System measurements from eastern Tibet and their implications for India/Eurasia intercontinental deformation, *J. Geophys. Res.*, *105*, 16,215–16,228.

Chevalier, M. L., P. Tapponnier, R. Ryerson, R. Finkel, J. Van Der Woerd, and Q. Liu (2004), Determination of the slip-rate on the Karakorum fault (Tibet) by dating of radioisotopes (^{10}Be), *Geophys. Res. Abstr.*, *6*, Abstract 05748.

Cobbold, P. R., and P. Davy (1988), Indentation tectonics in nature and experiment. 2. Central Asia, *Bull. Geol. Inst. Uppsala*, *14*, 143–162.

England, P., and G. Houseman (1986), Finite strain calculations of continental deformation: 2. Comparison with the India-Asia collision zone, *J. Geophys. Res.*, *91*, 3664–3676.

England, P., and P. Molnar (1997a), Active deformation of Asia: From kinematics to dynamics, *Science*, *278*, 647–649.

England, P., and P. Molnar (1997b), The field of crustal velocity in Asia calculated from quaternary rates of slip on faults, *Geophys. J. Int.*, *130*, 551–582.

England, P., and P. Molnar (2005), Late Quaternary to decadal velocity fields in Asia, *J. Geophys. Res.*, *110*, B12401, doi:10.1029/2004JB003541.

Flesch, L. M., A. J. Haines, and W. E. Holt (2001), Dynamics of the India-Eurasia collision zone, *J. Geophys. Res.*, *106*, 16,435–16,460.

Frank, F. C. (1972), Plate tectonics, the analogy with glacial flow, and isostasy, in *Flow and Fracture of Rocks*, *Geophys. Monogr. Ser.*, vol. 16, edited by H. C. Heard et al., pp. 285–292, AGU, Washington, D. C.

Heki, K., S. Miyazaki, H. Takahashi, M. Kasahara, F. Kimata, S. Miura, N. F. Vasilenko, A. Ivashchenko, and K. An (1999), The Amurian Plate motion and current plate kinematics in eastern Asia, *J. Geophys. Res.*, *104*, 29,147–29,156.

Houdry, F. (1994), Mécanismes de l'extension continentale dans le rift Nord-Baikal, Sibérie: Contraintes des données d'imagerie SPOT, de terrain, de sismologie et de gravimétrie, Ph.D. thesis, Univ. Pierre et Marie Curie-Paris 6, Paris.

Houseman, G., and P. England (1986), Finite strain calculations of continental deformation: 1. Method and general results for convergent zones, *J. Geophys. Res.*, *91*, 3651–3663.

Houseman, G., and P. England (1993), Crustal thickening versus lateral expulsion in the India-Asian continental collision, *J. Geophys. Res.*, *98*, 12,233–12,249.

Jade, S., B. Bhatt, R. Bendick, V. Gaur, P. Molnar, M. Anand, and D. Kumar (2004), GPS measurements from the Ladakh Himalaya, India: Preliminary tests of plate-like or continuous deformation in Tibet, *Geol. Soc. Am. Bull.*, *116*, 1385–1391.

Jiménez-Munt, I., and A. M. Negredo (2003), Neotectonic modelling of the western part of Africa-Eurasia plate boundary: From the Mid-Atlantic Ridge to Algeria, *Earth Planet. Sci. Lett.*, *205*, 257–271.

Jiménez-Munt, I., P. Bird, and M. Fernàndez (2001), Thin-shell modeling of neotectonics in the Azores-Gibraltar region, *Geophys. Res. Lett.*, *28*, 1083–1086.

Jiménez-Munt, I., R. Sabadini, A. Gardi, and G. Bianco (2003), Active deformation in the Mediterranean from Gibraltar to Anatolia inferred from numerical modeling and geodetic and seismological data, *J. Geophys. Res.*, *108*(B1), 2006, doi:10.1029/2001JB001544.

Khilko, S. D., R. A. Kurushin, V. M. Kotchetkov, L. A. Misharina, V. I. Melnikova, N. A. Gileva, S. V. Lastochkin, I. Baljinnyan, and D. Monhoo (1985), Strong earthquakes, paleoseismogeological and macroseismic data, in *Earthquakes and the Base for Seismic Zoning of Mongolia* (in Russian), *Trans. Jt. Sov.-Mongolian Res. Geol. Sci. Exp. 41*, pp. 19–83, Nauka, Moscow.

King, R. W., F. Shen, B. C. Burchfiel, L. H. Royden, E. Wang, Z. Chen, Y. Liu, X. Y. Zhang, J. X. Zhao, and Y. Li (1997), Geodetic measurement of crustal motion in southwest China, *Geology*, *25*(2), 179–182.

Kirby, S. H. (1983), Rheology of the lithosphere, *Rev. Geophys.*, *21*, 1458–1487.

Kirby, S., and A. Kronenberg (1987), Rheology of the lithosphere: Selected topics, *Rev. Geophys.*, *25*, 1219–1244.

Kogan, M. G., G. M. Steblov, R. W. King, T. A. Herring, D. I. Frolov, S. G. Egorov, V. Ye. Levin, A. Lerner-Lam, and A. Jones (2000), Geodetic constraints on the rigidity and relative motion of Eurasia and North America, *Geophys. Res. Lett.*, *27*, 2041–2044.

Kong, X., and P. Bird (1995), SHELLS: A thin-plate program for modeling neotectonics of regional or global lithosphere with faults, *J. Geophys. Res.*, *100*, 22,129–22,131.

Kong, X., and P. Bird (1996), Neotectonics of Asia: Thin-shell finite-element models with faults, in *Tectonic Evolution of Asia*, edited by A. Yin and T. M. Harrison, pp. 18–34, Cambridge Univ. Press, New York.

Lacassin, R., F. Valli, N. Arnaud, P. H. Leloup, J. L. Paquette, H. Li, P. Tapponnier, M.-L. Chevalier, S. Guillot, G. Maheo, and Z. Xu (2004), Large-scale geometry, offset and kinematic evolution of the Karakorum fault, Tibet, *Earth Planet. Sci. Lett.*, *219*, 255–269.

Lasserre, C., et al. (1999), Postglacial left slip rate and past occurrence of $M \geq 8$ earthquakes on the western Haiyuan fault, Gansu, China, *J. Geophys. Res.*, *104*, 17,633–17,652.

Lebedev, S., and G. Nolet (2003), Upper mantle beneath Southeast Asia from *S* velocity tomography, *J. Geophys. Res.*, *108*(B1), 2048, doi:10.1029/2000JB000073.

Lesne, O. (1999), Dynamique de l'extension intracontinentale dans le rift Baıuml;kal (Sibérie): Apport de mesures GPS et modèles numériques, Ph.D. thesis, Univ. de Nice-Sophia-Antipolis, Nice, France.

Levi, K. G., et al. (1995), Active Baikal tectonics, *Russ. Geol. Geophys.*, *36*(10), 143–154.

Li, S., and W. D. Mooney (1998), Crustal structure of China from deep seismic sounding profiles, *Tectonophysics*, *288*, 105–113.

Liu, Z., and P. Bird (2002a), Finite element modeling of neotectonics in New Zealand, *J. Geophys. Res.*, *107*(B12), 2328, doi:10.1029/2001JB001075.

Liu, Z., and P. Bird (2002b), North America plate is driven westward by lower mantle flow, *Geophys. Res. Lett.*, *29*(24), 2164, doi:10.1029/2002GL016002.

Lysak, S. (1992), Heat flow variations in continental rifts, *Tectonophysics*, *208*, 309–323.

Mériaux, A.-S., F. J. Ryerson, P. Tapponnier, J. Van der Woerd, R. C. Finkel, X. Xu, Z. Xu, and M. W. Caffee (2004), Rapid slip along the central Altyn Tagh Fault: Morphochronologic evidence from Cherchen He and Sulamu Tagh, *J. Geophys. Res.*, *109*, B06401, doi:10.1029/2003JB002558.

Mériaux, A.-S., et al. (2005), The Aksay segment of the northern Altyn Tagh fault: Tectonic geomorphology, landscape evolution, and Holocene slip rate, *J. Geophys. Res.*, *110*, B04404, doi:10.1029/2004JB003210.

Michel, G. W., et al. (2001), Crustal motion and block behaviour in SE-Asia from GPS measurements, *Earth Planet. Sci. Lett.*, *187*, 239–244.

Molnar, P., and Q. Deng (1984), Faulting associated with large earthquakes and the average of deformation in central and eastern Asia, *J. Geophys. Res.*, *89*, 6203–6227.

Molnar, P., and Gibson (1996), A bound on the rheology of continental lithJ.M. osphere using very long baseline interferometry: The velocity of South China with respect to Eurasia, *J. Geophys. Res.*, *101*, 545–553.

Molnar, P., and P. Tapponnier (1975), Cenozoic tectonics of Asia: Effects of a continental collision, *Science*, *189*, 419–426.

Molnar, P., and P. Tapponnier (1978), Active tectonics of Tibet, *J. Geophys. Res.*, *83*, 5361–5375.

Molnar, P., T. J. Fitch, and F. T. Wu (1973), Fault plane solutions of shallow earthquakes and contemporary tectonics in Asia, *Earth Planet. Sci. Lett.*, *19*, 101–112.

Molnar, P., B. C. Burchfield, Z. Zhao, K. Liang, S. Wang, and M. Huang (1987), Geologic evolution of northern Tibet: Results of an expedition to Ulugh Muztagh, *Science*, *235*, 299–305.

Mooney, W. D., G. Laske, and G. Masters (1998), CRUST 5.1: A global crustal model at 5° *times* 5°, *J. Geophys. Res.*, *103*, 727–747.

Moore, T. C., K. D. Klitgord, A. J. Golmshtok, and E. Weber (1997), Sedimentation and subsidence patterns in the central and north basins of Lake Baikal from seismic stratigraphy, *Geol. Soc. Am. Bull.*, *109*(6), 746–766.

Okal, E. (1977), The July 9 and 23, 1905, Mongolian earthquakes: A surface wave investigation, *Earth Planet. Sci. Lett.*, *34*, 326–331.

Paul, J., et al. (2001), The motion and active deformation of India, *Geophys. Res. Lett.*, *28*, 647–650.

Peltzer, G., and F. Saucier (1996), Present-day kinematics of Asia derived from geological fault rates, *J. Geophys. Res.*, *101*, 27,943–27,956.

Peltzer, G., and P. Tapponnier (1988), Formation and evolution of strike-slip faults, rifts, and basins during the India-Asia collision: An experimental approach, *J. Geophys. Res.*, *315*, 15,085–15,117.

Pollack, H. N., S. J. Hurter, and J. R. Johnson (1993), Heat flow from the Earth's interior: Analysis of the global data set, *Rev. Geophys.*, *31*, 267–280.

Prentice, C. S., K. Kendrick, K. Berryman, A. Bayasgalan, J. F. Ritz, and J. Q. Spencer (2002), Prehistoric ruptures of the Gurvan Bulag fault, Gobi Altay, Mongolia, *J. Geophys. Res.*, *107*(B12), 2321, doi:10.1029/2001JB000803.

Replumaz, A. (1999), Reconstruction de la zone de collision Inde-Asie. Etude centrée sur l'Indochine, Ph.D. thesis, Univ. Denis Diderot-Paris 7, Paris.

Ritz, J. F., E. T. Brown, D. L. Bourlès, H. Philip, A. Schlupp, G. M. Raisbeck, F. Yiou, and B. Enkhtuvshin (1995), Slip rates along active faults estimated with cosmic-ray-exposure dates: Application to the Bogd fault, Gobi-Alta, Mongolia, *Geology*, *23*, 1019–1022.

Ritz, J.-F., et al. (2003), Late Pleistocene to Holocene slip rates for the Gurvan Bulag thrust fault (Gobi-Altay, Mongolia) estimated with ^{10}Be dates, *J. Geophys. Res.*, *108*(B3), 2162, doi:10.1029/2001JB000553.

Robbins, J. W., D. E. Smith, and C. Ma (1993), Horizontal crustal deformation and large scale plate motions inferred from space geodetic techniques, in *Contributions of Space Geodesy to Geodynamics: Crustal Dynamics*, *Geodyn. Ser.*, vol. 23, edited by D. E. Smith and D. L. Turcotte, pp. 21–36, AGU, Washington, D. C.

San'kov, V. A., et al. (2002), On the estimation of rates of horizontal Earth crust movements of the Baikal rift system on the basis of GPS geodesy and seismotectonics, in *Tectonophysics Today* (in Russian), edited by V. N. Strakhov and Y. G. Leonov, pp. 120–128, United Inst. of the Phys. of the Earth, Russ. Acad. of Sci., Moscow.

Schlupp, A. (1996), Néotectonique de la Mongolie occidentale analysée à partir de données de terrain, sismologiques et satellitaires, Ph.D. thesis, Univ. Louis Pasteur, Strasbourg, France.

Sella, G. F., T. H. Dixon, and A. Mao (2002), REVEL: A model for Recent plate velocities from space geodesy, *J. Geophys. Res.*, *107*(B4), 2081, doi:10.1029/2000JB000033.

Shen, Z., C. Zhao, A. Yin, Y. Li, D. D. Jackson, P. Fang, and D. Dong (2000), Contemporary crustal deformation in east Asia constrained by Global Positioning System measurements, *J. Geophys. Res.*, *105*, 5721–5734.

Shen, Z., M. Wang, Y. Li, D. D. Jackson, A. Yin, D. Dong, and P. Fang (2001), Crustal deformation along the Altyn Tagh fault system, western China, from GPS, *J. Geophys. Res.*, *106*, 30,607–30,622.

Sherman, S. (1978), Faults of the Baikal Rift Zone, *Tectonophysics*, *45*, 31–39.

Socquet, A., G. Peltzer, and C. Lasserre (2005), Interseismic deformation along the central segment of the Altyn Tagh Fault (Tibet, China) determined by SAR interferometry, *Eos Trans. AGU*, *86*(52), Fall Meet. Suppl., Abstract G53A-0872.

Socquet, A., C. Vigny, N. Chamot-Rooke, W. Simons, C. Rangin, and B. Ambrosius (2006), India and Sunda plates motion and deformation along their boundary in Myanmar determined by GPS, *J. Geophys. Res.*, *111*, B05406, doi:10.1029/2005JB003877.

Tapponnier, P., and P. Molnar (1977), Active faulting and tectonics of China, *J. Geophys. Res.*, *82*, 2905–2930.

Tapponnier, P., and P. Molnar (1979), Active faulting and Cenozoic tectonics of Tian Shan, Mongolia, and Baykal regions, *J. Geophys. Res.*, *84*, 3425–3459.

Tapponnier, P., G. Peltzer, A. Y. Le Dain, R. Armijo, and P. Cobbold (1982), Propagating extrusion tectonics in Asia: New insights from simple experiments with plasticine, *Geology*, *10*, 611–616.

Tapponnier, P., F. J. Ryerson, J. Van der Woerd, A. S. Mériaux, and C. Lasserre (2001), Long-term slip rates and characteristic slip: Keys to active fault behaviour and earthquake hazard, *C. R. Acad. Sci.*, *333*, 483–494.

Thatcher, W. (2003), GPS constraints on the kinematics of continental deformation, *Int. Geol. Rev.*, *45*, 191–212.

Van der Woerd, J., F. J. Ryerson, P. Tapponnier, A.-S. Meriaux, Y. Gaudemer, B. Meyer, R. C. Finkel, M. W. Caffee, Z. Guoguang, and X. Zhiquin (2000), Uniform slip-rate along the Kunlun Fault: Implications for seismic behavior and large-scale tectonics, *Geophys. Res. Lett.*, *27*, 2353–2356.

Villaseñor, A., M. H. Ritzwoller, A. L. Levshin, M. P. Barmin, E. R. Engdahl, W. Spakeman, and J. Trampert (2001), Shear velocity structure of central Eurasia from inversion of surface wave velocities, *Phys. Earth Planet. Inter.*, *123*, 169–184.

Vilotte, J. P., M. Daignieres, and R. Madariaga (1982), Numerical modeling of intraplate deformation: Simple mechanical models of continental collision, *J. Geophys. Res.*, *87*, 19,709–19,728.

Wallace, K., G. Yin, and R. Bilham (2004), Inescapable slow slip on the Altyn Tagh fault, *Geophys. Res. Lett.*, *31*, L09613, doi:10.1029/2004GL019724.

Wang, Q., et al. (2001), Present-day crustal deformation in China constrained by Global Positioning System measurements, *Science*, *294*, 574–577.

Wright, T. J., B. Parson, P. C. England, and E. J. Fielding (2004), InSAR observations of low slip rates on the major faults of western Tibet, *Science*, *305*, 236–239.

Zhang, Q. Z., P. Vergely, and J. Mercier (1995), Active faulting in and along the Qinling Range (China) inferred from SPOT imagery analysis and extrusion tectonics of south China, *Tectonophysics*, *243*, 69–95.

E. Calais and L. Dong, Department of Earth and Atmospheric Sciences, Purdue University, West Lafayette, IN 47907-1397, USA.

M. Vergnolle, Laboratoire de Géophysique Interne et Tectonophysique, Maison des Géosciences, BP 53, F-38041 Grenoble Cedex 9, France. (mathilde.vergnolle@obs.ujf-grenoble.fr)